Development of lens-free dual-color fluorescence imaging device for Förster Resonance Energy Transfer (FRET) Imaging

---

FRET イメージング用レンズフリー ２色蛍光イメージングデバイスの開発

Hee Wan Shen

December 2019

NARA INSTITUTE OF SCIENCE AND TECHNOLOGY

GRADUATE SCHOOL OF MATERIALS SCIENCE

Acknowledgement

First of all, I would like to thank Professor Jun Ohta for providing me a chance to pursue my doctoral degree at the Nara Institute of Science and Technology (NAIST). Throughout my study, he offered me a lot of guidance and advice for my research, as well as offering chances to expand my knowledge and share it with others when the opportunities present themselves. Next, I would like to thank my supervisors, Professor Yukiharu Uraoka and Associate Professor Ken Hattori for giving me many useful insights on my research. I am also very grateful to Associate Professor Kiyotaka Sasagawa for teaching me a lot of useful technique that I required to complete my research, as well as providing me with many fruitful discussions whenever I am facing problem in my research, which helps me in setting the direction of my entire research. I would also like to thank Professor Takashi Tokuda (has been transferred to Tokyo Institute of Technology), Associate Professor Toshihiko Noda (has been transferred to Toyohashi University of Technology) and Assistant Professor Makito Haruta for providing me with technical support and advice on my research work throughout my study. I would also like to appreciate Ms. Ryoko Fukuzawa, our lab's secretary who always helps in managing paperwork for me, allowing me to allocate more time in my research work. I would also like to extend my acknowledgment to all lab members who provide help whenever I need, no matter it is related to works or personal issues. Special thanks also are given to Associate Professor Benoit Gosellin from University Laval, Canada for giving me an opportunity to have my internship in his lab.

During the internship period, he put me in charge of setting up a wet lab section in his lab to produce customized optical filter for his device. This allows me to apply the knowledge in the lab and elsewhere. Special thanks also addressed to Prof. Michiyuki Matsuda, our collaborator from Kyoto University. In this collaboration, I learnt about many new knowledge in biotechnology field and it would not been possible if I did not work on this collaboration project. I would like to thanks my lovely wife, who is also a Ph.D. student in the Division of Biological Science, NAIST. She is the one who encourages me to pursue my doctoral degree and supports me throughout the difficulties in my life. I would like to thank all my friends and Malaysian students at NAIST for helping me when I am in trouble. Last but not least, thanks to my family members who are always supportive and encouraging.

Contents

Chapter 1
Introduction

1.1 Lens-free imaging system

1.1.1 Overview

Recently, lens-free imaging system are gathering serious attention from various research group [1-13]. As its name suggested, lens-free imaging is an imaging system that does not include any lens in its design, as oppose to the traditional microscopic imaging device where lens play an important role in the imaging part [9]. Since no lens is used in a lens-free imaging system, the target image is now directly recorded on a digital image sensing array without being optically focused or magnified by a lens [9, 14]. In this way, the physical size of the imaging system can be significantly reduced without having to sacrifice its resolution. Moreover, by utilizing lens-free approach, the field-of-view (FOV) of the system can be increased and a more compact design of the system can be achieved [4, 7, 9].

The rapid improvement in lens-free imaging system was largely aided by the mass production low cost digital image sensor chips. These image sensor chips usually produced using complementary metal oxide semiconductor (CMOS) or charge-coupled device (CCD) technology and have small pixel size and large pixel counts on the chip. By pairing the lens-free imaging system with such digital image sensor chip and computer with sufficiently high performance central processing units (CPUs) and graphics processing units (GPUs), as well as

mature image reconstruction algorithm, this will open up various applications for the lens-free imaging system [9, 13].

1.1.2 Application of lens-free imaging system

In the field of bio-imaging, the optical microscope that was invented in the 17th century [5] and the fluorescence microscope that was invented in the 20th century [15] still remain as the most important visualization tools. However, due to its narrow FOV, large and bulky size, and high cost, conventional microscopy had become the bottleneck of in bio-imaging [4], especially for long-term cell imaging [16]. The rapid development of lens-free imaging device, however, opens up an alternative for bio-imaging research in a way that high resolution imaging is made possible in small area. For example, various research groups had successfully developed a small image sensor that can be used to observe cell growth, either to be placed in an incubator [6, 8]; acting as part of a smart petri dish that can grow cultured cell on it as well as capturing image of the cultured cell [3]; or even to be used as a real-time sensor under *ex vivo* conditions [12].

Other than that, lens-free imaging system can also be applied in *in vivo* researches, for example a small image sensor can be implanted with minimal invasiveness to the brain of rodents to observe their brain activity [17]; or the image sensor can be paired with on-chip LEDs to illuminate and detect light in deep biological tissues for optical therapy and diagnosis purposes [18] as well as to study optogenetics on small animals [19]. Last but not least, the

lens-free imaging system can also act as a small fluorescence microscope where it can do fluorescence imaging on cultured cell [20].

1.2 Förster resonance energy transfer (FRET)

1.2.1 FRET theory

In the year of 1940s, German physicist Thedor Förster discovered a photophysical mechanism of energy transfer which later named as FRET [21]. FRET described the process of two fluorescent molecules in close proximity interact with each other [22-24]. These two fluorescent molecules comprise of a donor and an acceptor molecule. When the donor fluorophore is excited by absorbing excitation light, an electron will be promoted to the excited state. As an electron in the excited state is not stable, it tends to drop back to the ground state by releasing the absorbed energy, usually in the form of fluorescence emission. In this case, no FRET activity is occurring as there is only fluorescence emission from the donor fluorophore [22].

On the other hand, when there is an acceptor fluorophore present in the close proximity, i.e.: within the electromagnetic field generated by the excited donor electron, typically within 1-10 nm, the energy can be passed to the acceptor through a non radiatively means, via long-range dipole-dipole coupling, where no fluorescence emission occurred during the energy transfer process [22, 23]. After that, the donor electron will drop back to the ground state, while

an electron from the acceptor will be promoted to the excited state. Finally, when the energy is released by the acceptor, fluorescence emission will usually occur. Due to resonance coupling between the fluorophores, during a FRET activity, the donor fluorescence emission will decrease, while the acceptor fluorescence emission will increase [22]. Figure 1.1 shows the summarized of FRET theory.

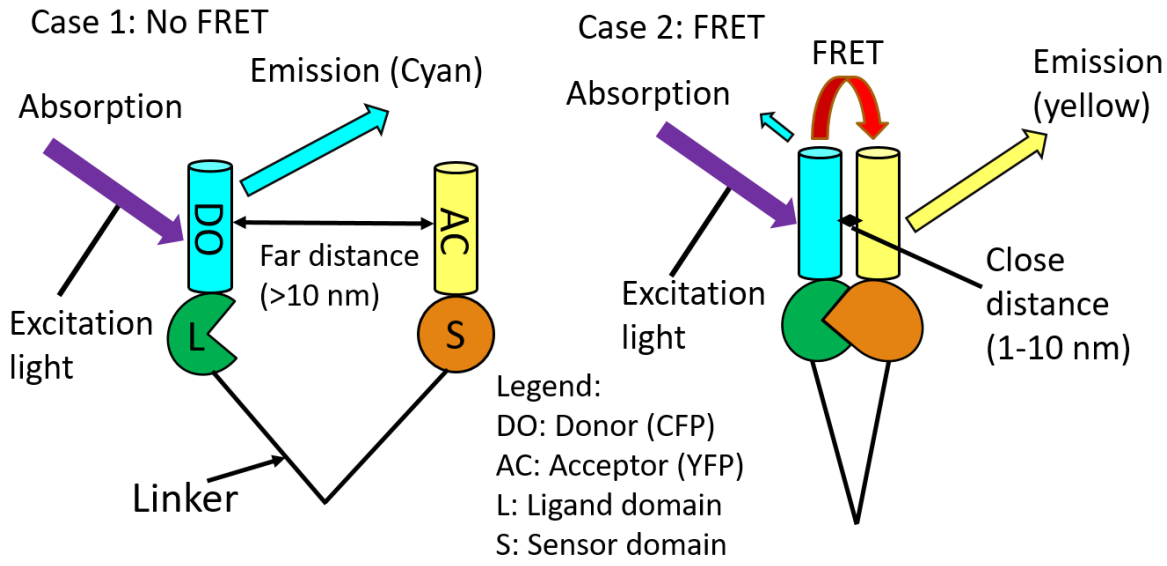

Figure 1.1: Summarized of FRET theory

1.2.2 FRET method

After its discovery, FRET began to be applied in biomedical researches around 1970s [22]. However, FRET's application actually flourishes shortly after the successfully cloning of green fluorescent protein (GFP) and the generation of various mutant fluorescent protein of various colors from GFP, for example the cyan fluorescent protein (CFP) and yellow fluorescent protein

(YFP) [25]. This fluorescent protein mutant derived from GFP form a donor and acceptor pair of FRET that can be used to detect intramolecular interaction within living cells [22].

In most of the researches involving FRET, FRET efficiency is determined and later used to deduced the intramolecular interaction. The FRET efficiency is the efficiency of energy transfer between donor and acceptor. Since FRET can only occur within the electromagnetic field generated by the excited electron and the electromagnetic field strength decreases with increasing distance, hence it is deduced that the FRET efficiency should be inversely proportional to the distance between the two fluorophores [22]. As stated by Förster, the FRET efficiency, E, is given by the following equation:

$$E = \frac{{R_0}^6}{R^6 + {R_0}^6} \quad (1)$$

where R is the physical distance between the donor and the acceptor, and R_0 is a term known as the Förster distance, where it is a characteristic distance for a particular fluorophore pair at which the FRET efficiency is equal to half [22]. For most FRET pair, the R_0 value lies somewhere between 2 and 8 nm [24]. In a simpler term, the FRET efficiency is depending on the inverse of 6th power of the distance between the fluorophores.

1.2.3 Advantages of FRET method

First of all, as stated previously, FRET efficiency is inversely proportional to the 6th power of the distance between fluorophores, it is highly sensitive to small changes in distance. Hence,

FRET method has been extensively used as a “ruler” to measure intermolecular and intramolecular distances [26]. Moreover, as FRET method only sensitive for flurophores that lies within a short distance, i.e.: around 2-8 nm, this distance is comparable to the separation between biomolecules. This make FRET method suitable to detect the intermolecular interactions [22].

Other than that, as most organic materials generally will not disturb the electromagnetic field, FRET method can be used to measure the distance between two fluorophores even though there is a physical blockage, e.g.: separated by the lipid bilayer. At the same time, cultured cells and thin tissues samples also transparent to visible light, fluorescence excitation and detection can be easily applied on many biological researches [22]. Last but not least, FRET method is noninvasive and long lasting. Unlike various biochemical methods, there is no need for the target molecules to be isolated. The use of fluorescent proteins allows the fluorophore labeling to be carried out at DNA level and studies can be carried out on the developing cells. By applying this on transgenic animals, FRET can even be used to study the protein-protein interaction throughout the lifespan on the transgenic animals [22].

1.2.4 FRET’s applications, its impact, and its bottleneck

Since the successful cloning of GFP and the generation of its mutants fluorescent proteins, FRET method had been applied in various researches, particularly in cell signaling and

biochemistry field [22]. For example, FRET had been applied to study the spatiotemporal dynamics of GTPases [27], kinase [28], and protein [29]. Other than that, FRET can also be applied to study cancer development [30] and monitor cancer related gene activity [31]. Moreover, it can also be applied in medicine development by studying the interaction between the targets after the medicine is given [32]. The developments in the aforementioned research can lead to improved knowledge of various diseases such as cancer. Subsequently, a possible method of reversing the development of such diseases might also be developed.

Although FRET method has been successfully applied to various research, most of it are application on *in vitro* studies. Although FRET expressing transgenic animal had been successfully breed, it is still being used in ex vivo experiment where the animal need to be anesthetized and some of the organ, for example the small intestine being pull out from its body to carried out the experiment [33, 34]. *In vivo* experiment on the transgenic animal still have not successfully conducted yet, mostly due to limitation in the equipment. Most of the researches on FRET are carried out using fluorescence microcopy method where the microscope itself is too big and cannot be inserted into the body of the transgenic animal for *in vivo* studies. However, by using a lens-free imaging system, an image sensor capable of observing *in vivo* FRET activity on transgenic animal can be developed.

1.3 Purpose of this research

In this research, an image sensor capable of observing FRET activity from CFP and YFP pair is fabricated. In order to do so, filters that are able to transmit fluorescent light from the fluorescent protein pairs and block excitation light at the same time are determined. Then, image sensor attached with the selected filters is fabricated and tested in an *in vitro* FRET experiment to make sure that it is capable of observing FRET activity.

After the functionality of the image sensor had been confirmed, a wireless module for the image sensor is developed. This wireless module allows the image sensor to communicate with the computer without being limited by the wire. By implanting the image sensor with the wireless module attached to it on the body of small animal, the animal can roam freely during an *in vivo* FRET imaging experiment.

1.4 Thesis outline

This thesis is separated into five chapters and the entire thesis describe the basic idea of fabricating a wireless CMOS image sensor for FRET imaging.

In this chapter, lens-free imaging system and FRET are described. Then the purpose of this research is explained.

In Chapter 2, discussion are made regarding the tools that can be used to study FRET. The advantages and disadvantages of these tools are also discussed.

In Chapter 3, the main structure of the lens-free imaging system is described. This include the image sensor chip, filters and other optical components. The fabrication process of the lens-free imaging system is also demonstrated. Also, the results on filters performance, image sensor performance, FRET experiment are displayed and discussed.

Chapter 4 describe the wireless module that will be coupled the imaging system. This include the structure of the wireless module, the program that runs the module and the imaging software that reconstruct the image obtained by the image sensor.

Last but not least, Chapter 5 summarizes the results and conclusions on this research is made. Future direction of this research is also made here.

Chapter 2

FRET Imaging Systems: Strengths and Limitations

2.1 Overview

FRET is a technique that can be applied to study the interactions between signaling molecules by detecting the emitted fluorescence. However, some imaging system must present during the experiment in order to capture the emitted fluorescence. In this chapter, the strengths and limitations of FRET imaging systems are discussed.

2.2 FRET imaging system – Fluorescence microscopy

2.2.1 The role of fluorescence microscopy in various FRET researches

Until today, fluorescence microscopy remain as one of the most commonly used tools for bio-imaging. Commonly used fluorescence microscopy in FRET research are confocal, wide-field and two photon microscopy and they contribute significantly toward FRET imaging experiment.

In order to carry out *in vitro* FRET imaging to study spatiotemporal dynamics of signaling molecules, the sensor and ligand domains (in more general terms, the donor and acceptor pair) of the signaling molecules have to be determined. Then, polymerase chain reaction (PCR) is carried out to clone the sensor and ligand domains and tag them with the fluorescent protein pairs. The sensor and ligand domains that are tagged with fluorescent protein pairs is now called

the FRET biosensor. Next, transfection is carried out to introduce the FRET biosensor into cultured cells. This cultured cell is then grow on a glass bottom dishes in a CO2 incubator. Further details regarding the bio-engineering process to produced the FRET biosensor can be found in [35]. Lastly, when the cells are ready for FRET imaging, images will be captured using fluorescence microscope to collect the required data.

The usage of fluorescence microscope is proved to be a huge success as high-resolution images with high signal-to-noise ratio can be obtained. Moreover, *in vitro* FRET imaging can be applied to various signaling molecules, for example GTPases, kinase, and protein and study their spatiotemporal dynamics. However, no conclusion can be drawn on how these signaling molecules works in an intracellular network. This is because all the signaling molecules in a living object might act cooperatively or counteractively with one another, as oppose to the *in vitro* study, where only one signaling molecule pairs are present. Thus, there is a need to study FRET activity of a living organism. With this goal in mind, transgenic mice that stably expressing FRET biosensor (FRET mouse) was created. Now, instead of observing FRET activity on a pair of signaling molecules, observation is carried out on an organ of the mouse instead, where it consists of various signaling molecules. In this way, how various signaling molecules interact with each other in an intracellular network can be studied [33, 34]. By using the FRET mouse and two-photon excitation microscopy, live imaging of protein kinase activity and time-lapse imaging of neutrophil recruitment to inflamed intestines of the FRET mouse can

be carried out. In this way, one can observe the interaction between various signaling molecules in the inflamed intestine of the FRET mouse when they try to recruit neutrophil to inflamed intestine in an act to try to cure it. However, these experiments was carried out with the FRET mouse anesthetized before its intestines can be pulled out from its body during a surgery. Then, two-photon excitation microscopy is used to collect the required data. Lastly, the FRET mouse is being sacrificed after the experiment [33, 34]. Although *in vivo* FRET imaging can be carried out on living animal in such way, it is in a relatively short period, i.e. in terms of hours. No long term *in vivo* FRET imaging can be carried out in this way as the mouse will die soon due to heavy injury on its body.

2.2.2 The pros and cons of fluorescence microscopy

Section 2.2.1 shows that the development of researches involving FRET technique is made possible with fluorescence microscopy at their disposal. Although different fluorescence microscopy might be used under different conditions, they all works in a similar way and have a few similar advantages. Like a normal microscope, lenses is utilized in the design of the fluorescence microscope. This allows the observation target to be magnified a number of times depending on the total power of the lenses in its design. This allows the fluorescence microscope to acquire high contrast and high resolution images and the observation can be carried out at a distance away from the target, depending on the focal length of the lenses in

use. The quality of the images taken by the fluorescence microscope can be further enhanced by removing out of focus images and "stacking" multiple images to produce high quality images [36]. Next, the fluorescence microscopes are highly sensitive imaging system with the use of high sensitive detector and lenses. This can reduce the data acquisition time and allow some of the short-lived fluorescence to be captured.

However, the fluorescence microscopy are not perfect. There are several disadvantages of the fluorescence microscopy that halted the further development of FRET application. First of all, the fluorescence microscopy required precise focus in order to obtain high quality images. This could be easily achieved under an *in vitro* or *ex vivo* condition, but difficult under *in vivo* condition. During an *in vivo* experiment, even the slightest movement from the host, for example from breathing and heartbeat can easily cause the fluorescence microscope to lose focus and derived serious errors in the data. Moreover, current *in vivo* experiment involve surgery on the host to drag its organs out from its body and data acquisition is carried out using the fluorescence microscope. In this situation, the host will soon die due to the heavy injury to its body and long term imaging (in terms of days or weeks) is not possible. Furthermore, the host need to be anesthetized throughout the experiment to keep the host fixed to a certain position. This step is to make sure the fluorescence microscope will not lose focus and to make sure the host will not move around and accelerate its death before the experiment ended since its organ is being pulled out of its body. In this case, imaging of freely moving animals using

fluorescence microscopy in *in vivo* experiment is hardly possible.

Other than that, there is a need to conduct long term FRET imaging experiment, preferably on free moving, stress free animals as it might explains many unanswered biomedical phenomena in living body, for example the cancer dormancy [37]. However, the big and bulky nature of a fluorescence microscope simply make it impossible to mount it on a host animal to carry out such experiment. Hence, there is a need to develop a small, implantable device with low invasiveness to carry out this task.

2.3 FRET imaging system – Miniature on-chip/ fiber-based FRET imaging system

2.3.1 The roles of miniature imaging system for fluorescence/ FRET imaging

To date, application of miniature imaging system on FRET imaging are very limited, probably due to technical difficulties such as two different fluorescence need to be detected individually and simultaneously, autofluorescence, low signal-to-noise ratio due to detector and optical noise, photobleaching, spectral bleedthrough signal and contamination of spectral crosstalk [36, 38]. To date, no implantable chip-based image sensor that can be used for *in vivo* FRET imaging purpose was reported. Nevertheless, Chai *et al.* successfully combined a miniature fiber optic spectrometer and a wide-field fluorescence microscope for spectral measurement of FRET in single living cells. With this design, a complete FRET quantification

measurement can be completed in 1-2s [38]. Although this is neither a miniature design where the whole system can be mounted on host animal, nor it is carried out on lab animals, this fiber based system opens up a possibility where similar system with implantable scale can be created and with the detector side implanted on the body of lab animals in the future.

Although miniature on-chip or fiber-based FRET imaging system are not yet widely available, similar systems had been successfully applied on fluorescence imaging. For example, Ohayon *et al.* presented a lens-less micro-endoscope that utilized an ultra-thin multi-mode optical fiber to capture deep brain fluorescence of GCaMP mouse with micron-scale resolution [39]. On the other hand, Papageorgiou *et al.* demonstrated that a small CMOS image sensor can be implemented to detect fluorescence emitted by cancer cell in real time and with high sensitivity [12]. With these success presented, it is only a matter of time where one can overcome the technical difficulties and create an on-chip or fiber-based FRET imaging system that can detect two different fluorescence simultaneously and individually in the future. In fact, a lens-free CMOS image sensor that is capable of detecting two different fluorescence from two fluorescent microbeads simultaneously had been successfully developed [40]. This shows that it will not be long when a lens-free imaging device that can be used for *in vivo* FRET imaging can be successfully developed.

2.3.2 The pros and cons of miniature on-chip/ fiber based fluorescence imaging system

Since on-chip/ fiber-based FRET imaging system are not vastly available, this section will discuss working principle of an on-chip image sensor, as well as the pros and cons of on-chip/ fiber-based fluorescence imaging system instead.

The on-chip imaging system utilized lensless imaging and sensing technique to acquire image. In this technique, the diffraction pattern resulting from an object, for example fluorescence in our case, will be recorded directly on a digital image sensor array (CMOS or CCD) without being optically focus or magnified by lenses. Then, this diffraction pattern will be reconstructed by using computer to form an "image" of the object [9]. This means that the observation target will be in direct contact with the sensing array of the image sensing system and this allow the imaging system to have wider field-of-view compared to the fluorescence microscope, since the image can be directly convey onto the sensing region of the imaging system. The spatial resolution of the on-chip imaging system will depend on the pixel size of the sensing region of the imaging system. To date, the smallest pixel size of a CMOS imager reported is with a size of 2.8 μm, equipped on an image sensor with active array size of 1280x960 [41].

By using lens-free imaging approach, the miniature fluorescence imaging system can be designed to be very small in size and low in weight. This allows its detector to be implanted into the body of small host animal with minimal invasiveness while the rest of the system can

be mounted on the body of the host animal without causing extra burden that will hinder the movement of the host animal [19]. Moreover, recent development in technology allow the production of device with compact hardware geometry, which means that more electronics parts can be added to the system with minimal increase in size and weight. This can potentially lead to the design of an automated imaging system. Next, the development in CMOS and CCD technology also permit real time measurement to be done with sufficiently high sensitivity [10, 42].

Although a miniature fluorescence imaging system have many advantages, it also have many limitations. For example, high background noise which in turn will lead to low signal-to-noise ratio often hamper its performance. Other than that, the image resolution obtained by the miniature fluorescence image sensor are limited by its size. This is because the resolution are depending on the number of pixels on the sensor and one need to sacrifice the size in trade of higher resolution. Last but not least, the small size of the imaging system also limited the information that can be obtained from a single device as some event might happened just outside the sensing region of the sensor. This might caused some precious information lost during the experiment [42].

Chapter 3
Dual-color CMOS Image Sensor with Hybrid Filter for FRET Imaging

3.1 CMOS Image Sensor

3.1.1 Overview

CMOS image sensor were generally known around mid 1960s but failed to compete with CCDs that are invented in 1970, largely due to poor performance and large pixel size at that time. It was until early 1990s that major breakthrough happened in CMOS technology that made it gain several advantages compared to CCDs [43]. For example, CMOS image sensor have lower power consumption and lower production cost compared to CCDs [43-45]. It's on chip functionality and compatibility allow it to be fabricated in a very small size. Moreover, by adding amplifier to the first generation passive pixel CMOS array, its signal-to-noise (SNR) ratio improve significantly. Therefore, sensors that implement a buffer, which acts as a simple source follower, have been known as active pixel sensor (APS), which is the second generation of CMOS image sensor [43]. The second generation CMOS image sensor have lower noise, higher speed and higher resolution [43-45]. These features made CMOS image sensor suitable to be applied in biomedical devices, for example implantable device for retinal prosthesis and deep brain fluorescence imaging [46]. In the field of biomedical imaging, many research group had successfully develop their own CMOS imaging device for single fluorescence detection

purpose [7, 11, 47, 48]. However, the application of similar image sensor for FRET imaging, which required simultaneous detection of two different fluorescence still remain unexplored. Hence, a CMOS image sensor that are capable of visualizing FRET activity as a developed device will be presented in this research.

3.1.2 CMOS image sensor chip design

In order to detect the fluorescence emitted as a results of FRET activity, some kind of detector must be used. In this work, a CMOS image sensor chip is being used as that detector. The image sensor chip is designed and fabricated using 0.35 μm 2-poly 4-metal standard CMOS technology (AMS). The sensing region is made up of an array of 60 × 134, three-transistor active pixel sensors, each with a size of 15 × 15 μm^2. Further details of the image sensor's specifications are listed in Table 3.1 and a microscope image of the image sensor chip is shown in Figure 3.1. The photodiodes occupied most of the area of the chip, while the four squares near the bottom are the bonding pads. These pads are connected to the clock signal (input signals), VDD (positive terminal), GND (ground terminal), and output (output terminal) on the control board.

Table 3.1: Specifications of image sensor

Process		0.35 μm 2-poly 4-metal standard CMOS process
Supply voltage (V)		3.3
Chip size (mm^2)		1.05 × 2.70
Pixel	Type	Three-transistor active pixel sensor
	Size (μm^2)	15 × 15
Pixel array size		60 × 134
Photodiode type		N-well/P-Substrate
Fill factor (%)		61.2

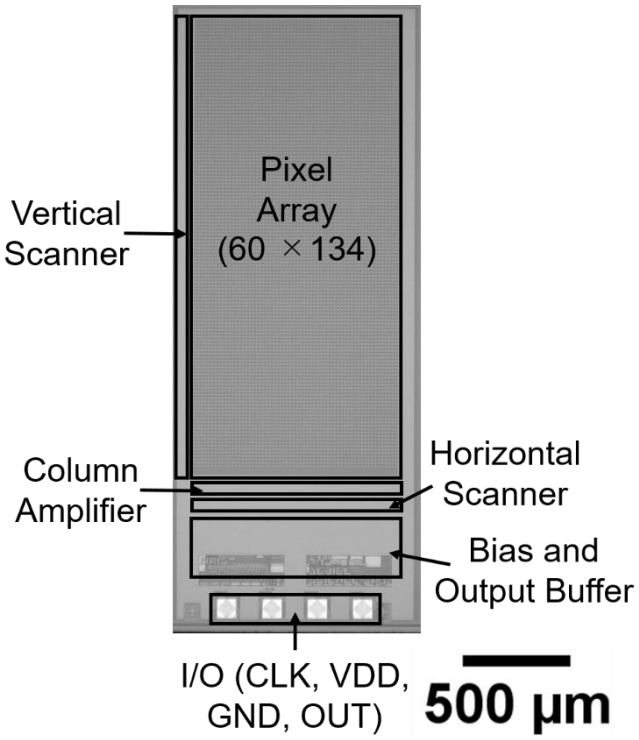

Figure 3.1: Microscope image of the image sensor chip.

For this image sensor, the saturation voltage occurs at around 800 mV, while the noise level of this sensor is at around 0.7 μV, hence making the dynamic range of the image sensor to be at around 60 dB.

As the detectors are Si photodiodes, they will detect photons of all wavelengths from the visible to near-infrared range. Hence, additional filters must be added to the image sensor to allow it to selectively detect target fluorescent light from the fluorescent protein pairs. In addition, the filters are also responsible for blocking excitation light to prevent it from reaching the photodiodes. The required performance of the filters needed will be explained in details in the next section.

3.2 Filters design

3.2.1 Filters selection criteria

To choose the best filters for our purpose, a few criteria must be fulfilled. First, all the filters must be able to transmit the target fluorescent light. In our work, the target FRET probe comprises two fluorescent proteins: an enhanced cyan fluorescent protein (ECFP, hereafter CFP) [49] and a yellow fluorescent protein for energy transfer (Ypet, hereafter YFP) [49]. The fluorescence emission originates from the CFP, with a peak near 474 nm, and the YFP, with a peak near 530 nm. Next, the filters should also be able to block the excitation light to prevent it from being detected by the photodiodes. This is crucial because the excitation light is very strong and it will saturate the image sensor if not treated properly. Moreover, leaked excitation light will considerably increase the photon shot noise when the signal is weak, as the photon shot noise is given by the square root of the signal intensity. Figure 3.2 shows the excitation

and emission spectrum of ECFP and Figure 3.3 shows the excitation and emission spectrum of Ypet.

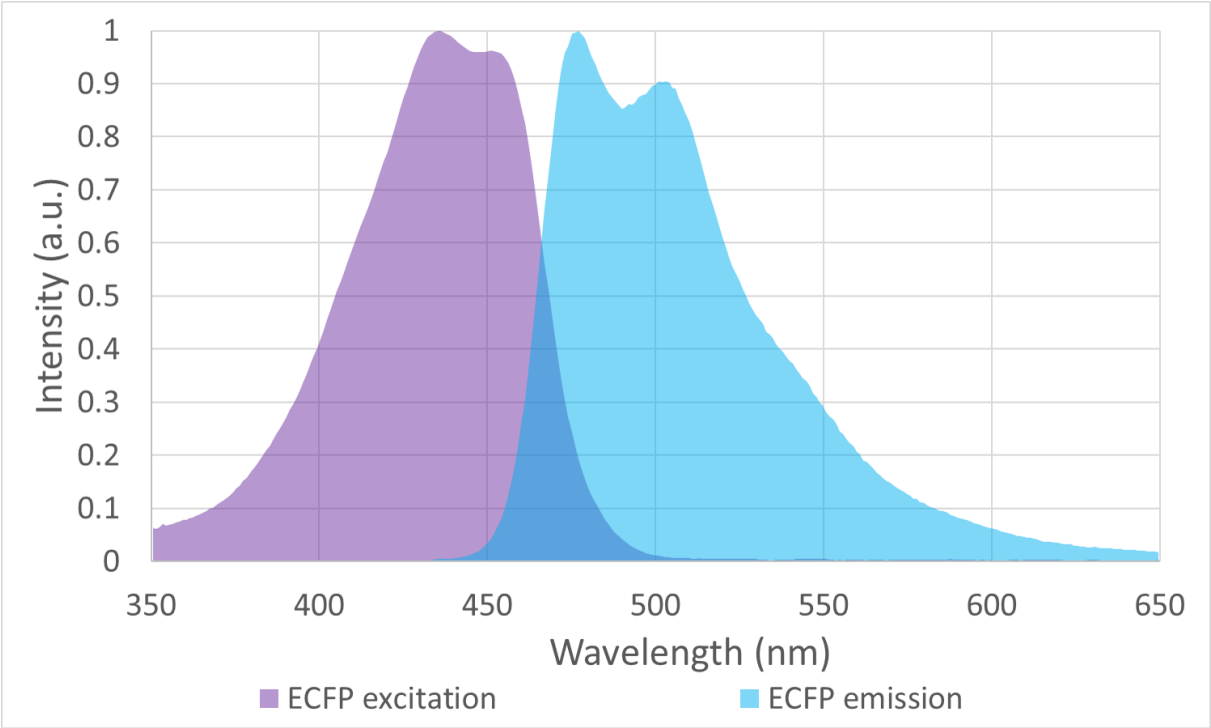

Figure 3.2: Excitation and emission spectrum of ECFP

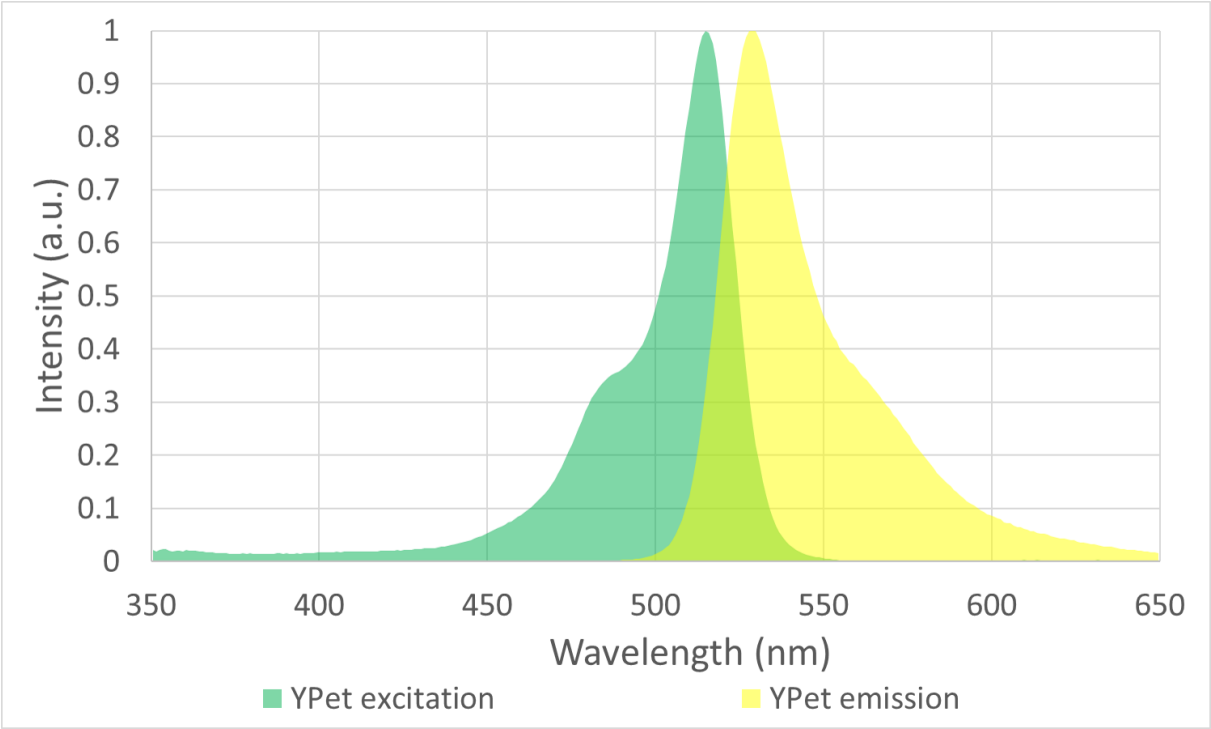

Figure 3.3: Excitation and emission spectrum of Ypet

To initiate the FRET activity for the CFP and YFP pair, a 435 nm excitation light is chosen as it is the peak excitation wavelength for CFP. Hence, the filters must show a high extinction ratio near this wavelength. Lastly, the filters also should not emit strong fluorescence. As the autofluorescence emitted by the filters is normally outside the rejection band of the filters, this fluorescence will be detected directly by the image sensor in a lens-free design because the filters are in the vicinity of the sensor. This situation is not desirable as it will affect the results of experiments.

3.2.2 Interference filter vs. absorption filter

The interference filter and absorption are the most commonly used as an emission filter for

fluorescence imaging. These filters will remove excitation light and transmit the target fluorescence. However, both kind of filters have their own advantages and disadvantages.

The interference filters are created by stacking multiple layers of dielectric with difference refractive indices. Unwanted wavelength of light will be rejected reflecting it away at a certain layer of dielectric and the targeted light will pass through the filter. In this way, interference filter with a very steep rejection band edge with high extinction ratio can be formed through precise fabrication process. Moreover, since excitation light are not absorbed by the interference filter, auto-fluorescence are normally not detected. However, the transmission spectrum of the interference filter will shift if the incident light is not normal. This is quite a drawback since the excitation light might be randomly scattered by an observation target, such as cells or microbeads during a fluorescence imaging experiment and the scattered excitation light is no longer normal. This will cause the interference filter to transmit the scattered excitation light instead of removing it. Furthermore, in most cases, the intensity of the scattered light component of the excitation light will still be much stronger than that of the target fluorescence, and thus this component cannot be ignored during fluorescence imaging [11].

On the other hand, the absorption filter, which used dyes or pigments to absorb light at specific wavelengths, it will absorb light coming from all direction. However, some of the absorbed excitation light will be re-emitted as the auto-fluorescence of the filter. This scenario is not preferable as it will affect the results of the experiment [11]. Moreover, the rejection band

of an absorption filter is broader than that of interference filter. This, in some case, will affect the performance of the absorption filter.

3.2.3 Hybrid filter

Since both the interference filter and absorption filter have their own advantages and disadvantages, a hybrid filter form by combining both filters should create a high-performance filter with the pros of both filters and none of the cons. This can be done by sandwiching the interference filter and the absorption filter between a high-resolution fiber optic plate (FOP) (J5734, Hamamatsu Photonics). The FOP is used here so that the combination of both filters can be carried out without decreasing their spatial resolution. The FOP is consists of multiple micro optical fiber where each micro optical fiber has a diameter of 3 μm. This allows the FOP to directly convey light from its input surface to its output surface without needing a focal length. Hence, the FOP is very suitable to be used in compact optical design.

By placing the interference filter on the top, it will cut down most of the excitation light coming from the normal direction. Some of the excitation light might still pass through the interference filter together with the scattered excitation light, but their intensity is considerably lower compared to the excitation light. These components of excitation light that passes through the interference filter will then be absorbed by the absorption filter. Since the absorption filter only absorb low intensity excitation light, it will produce low to none auto-fluorescence. Figure

3.4 shows the working principle of the hybrid filter. As this only shows the working principle of the most basic hybrid filter, multiple layers of interference filter and absorption filter can be added to form a more complicated hybrid filter when needed.

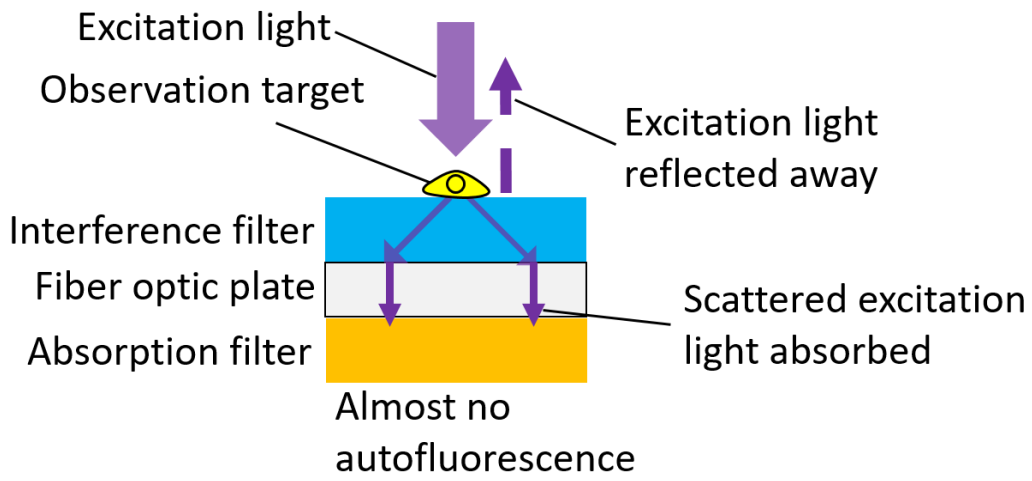

Figure 3.4: Hybrid filter's working principle

3.2.4 Hybrid filter structure for our device

By considering the criteria stated previously, a hybrid filter is developed for our device. The hybrid filter structure of our device consists of two main layers. The lower layer is a selective detection layer that consists of alternate lines of blue and yellow-green absorption filters. In contrast, the upper layer is the excitation light removal layer. This layer consists of a 460 nm long-pass interference filter, a fiber optic plate (FOP), a 550 nm short-pass interference filter (the long-pass and short-pass interference filters form a bandpass interference filter), FOP, a yellow absorption filter (FDB-003) and FOP from the top to the bottom of the layer. This filter

structure is illustrated in Figure 3.5.

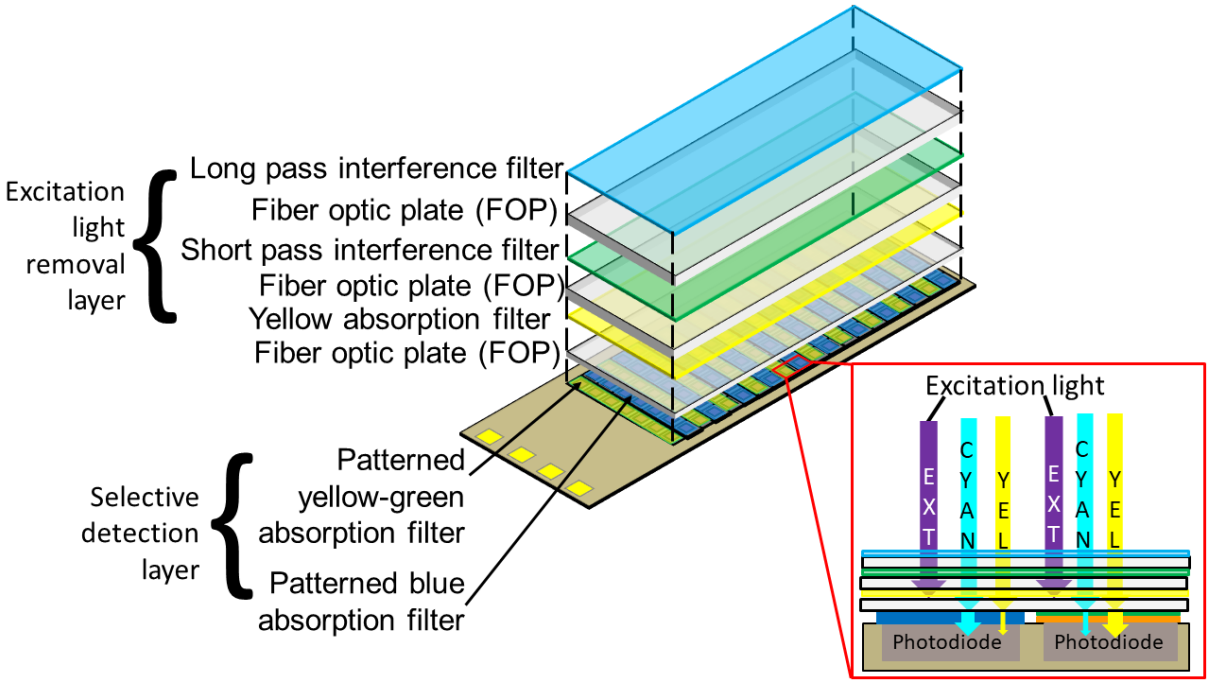

Figure 3.5: Illustration of the filters applied to the image sensor.

As stated above, the excitation removal layer which is made up of a hybrid filter will remove the unwanted excitation light and transmit the target fluorescent light. The transmission spectra of the filters used in the excitation light removal layer with respect to the emission of the fluorescent proteins are shown in Figure 3.6.

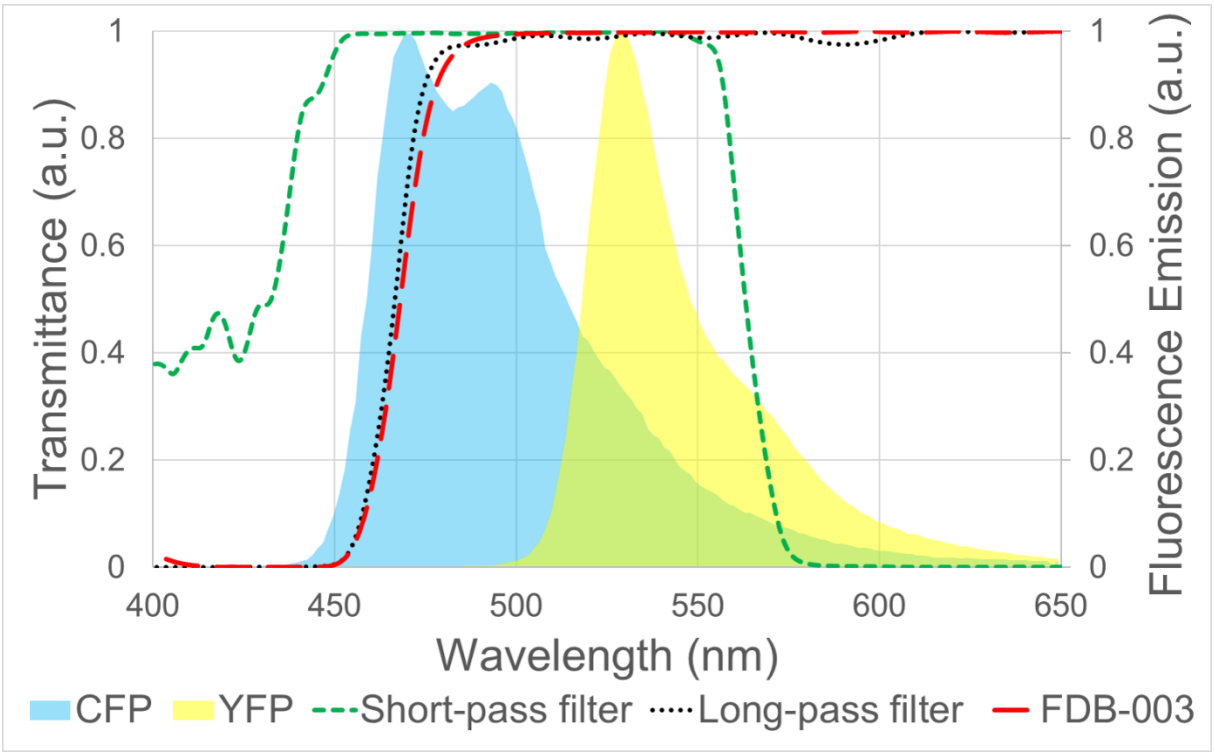

Figure 3.6: Transmission spectra of the filters used in the excitation light removal layer with respect to the emission of the fluorescent proteins.

Here, the transmission spectrum of each individual filter are measured by using a spectrophotometer (JASCO V-670 UV-VIS-NIR Spectrophotometer). The filters are casted on microscope cover glass (Matsunami glass) according to the condition stated in section 3.3.1 and 3.3.2. On the other hand, the fluorescence emission spectrum for CFP[49] and YFP[49] are obtained from their database. According to Figure 3.6, the bandpass interference filter and the yellow absorption filter are both capable of blocking excitation light near 435 nm and allow cyan and yellow fluorescent light from the CFP and YFP, respectively, to pass through them, hence fulfilling our filter selection criteria.

Next, the target fluorescent light will then be further selectively detected by the alternate

lines of blue and yellow-green absorption filter which are directly coated on the photodiodes. The blue absorption filters are responsible for transmitting cyan fluorescent light and absorbing yellow fluorescent light. The opposite applies for the yellow-green absorption filters. In this way, two different types of filters will coat alternate neighboring pixels. This makes it possible to selectively detect of two different fluorescent lights in the same area. The transmission spectra of the filters used in the selective detection layer with respect to the emission of the fluorescent proteins are shown in Figure 3.7.

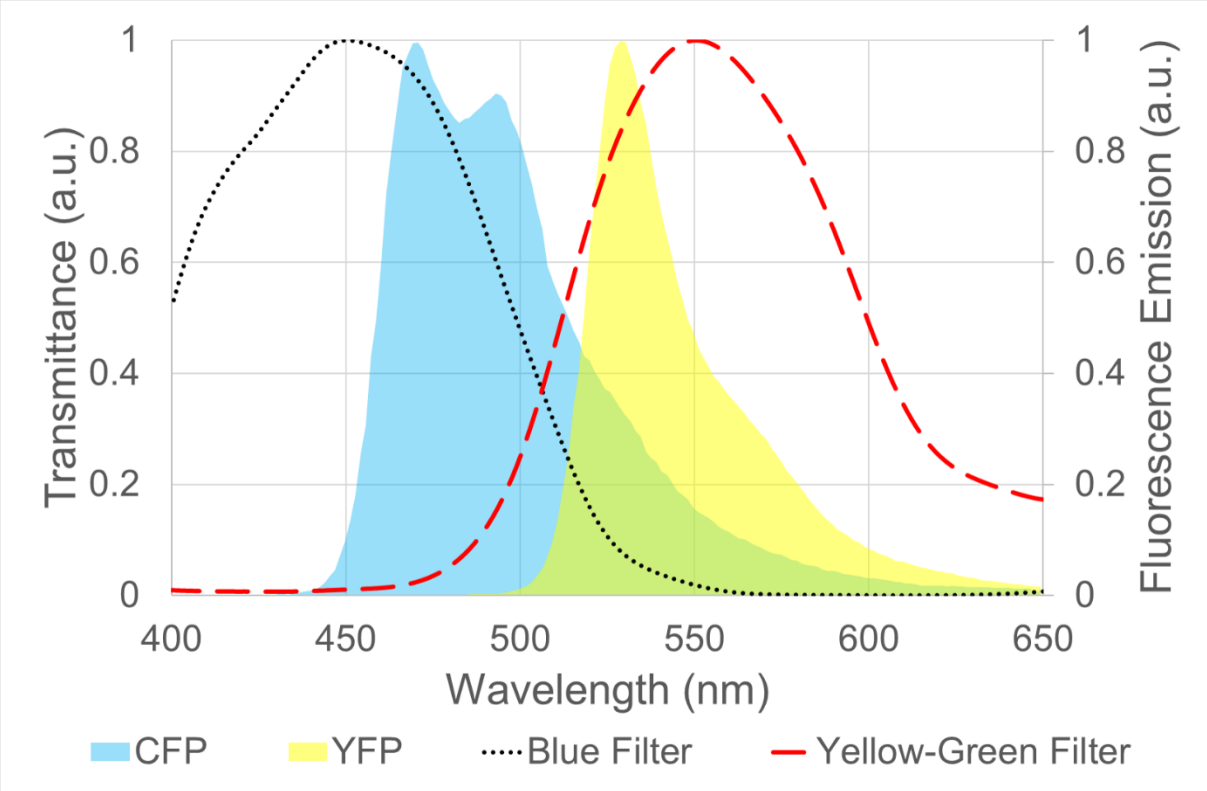

Figure 3.7: Transmission spectra of the filters used in the selective detection layer with respect to the emission of the fluorescent proteins.

Similar as previous, the transmission spectrum of each individual filter are measured by using a spectrophotometer (JASCO V-670 UV-VIS-NIR Spectrophotometer). The filters are casted on microscope cover glass (Matsunami glass) according to the condition stated in section 3.3.1 and 3.3.2. According to Figure 32.7, the blue absorption filter will transmit most of the cyan fluorescent light emitted by the CFP and block most of the yellow fluorescent light emitted by the YFP. The opposite applies to the yellow-green absorption filter. This shows that the blue and yellow-green filters are capable of selectively detecting fluorescent light in the desired region of the image sensor when they are coated on the sensor.

In theory, although the filters in the selective detection layer can be design in a way that it only detect individual fluorescence only, instead of having an overlapping region with the other fluorescence. To achieved this, the filter to have a cutoff wavelength around 500 nm. For example, the filter responsible to detect the cyan fluorescence is made up of short pass filter with cutoff wavelength of 500 nm and the filter responsible to detect yellow fluorescence is made up of long pass filter with cutoff wavelength of 500 nm. However, in actual case, this is almost impossible due to a few reasons. First of all, filter with such performance can only be achieved by using an interference filter as the rejection band of absorption filter is very broad. However, as the fluorescence emitted mostly comes from various direction. The angle shifting phenomena on the interference filter will cause the filter that responsible to detect yellow fluorescence detect the cyan fluorescence instead. The angle shifting phenomena will caused

the filter responsible to detect the cyan fluorescence to cut off a larger amount of cyan fluorescence as the ECFP have a secondary emission peak around 490 nm and the angle shifting phenomena will caused the filter to block this wavelength instead. Next, the quantum yield of CFP is larger compared to that of YFP. Even though we design an optical filter with cutoff wavelength at 500 nm, the filter responsible to detect the yellow fluorescence will still be dominated by the cyan fluorescence at that region. Lastly, in order to selectively detect cyan and yellow fluorescence from the same source, two neighboring pixel in y-direction need to be coated with two different filters. As the pitch size of our pixel is 15 μm, the production of interference filter with such low pitch size is very difficult. Even if it is possible to fabricate interference filter with such low pitch size, assembly of the FOP coated with such interference filter onto the designated pixel on the image sensor is also almost impossible to be carried out.

3.3 Fabrication process

3.3.1 Fabrication of the selective detection layer

First, a yellow dye solution is prepared by mixing a yellow dye powder (Valifast Yellow 3120, Orient Chemical Corporation) with cyclopentanone (120-92-3, Tokyo Chemical Industrial Corporation) and epoxy resin (GA, Cannon Chemical) with a weight ratio of 1:8:1. Then, some of the yellow dye solutions is added dropwise to the image sensor, and spin-coated at a speed of 1500 rpm for 30 s using a spin coater. The dye is then subjected to 60 s of UV

illumination, followed by baking at 150 °C under vacuum for 45 min. This forms a layer acting as a yellow filter on the image sensor. After that, some green dye (SG-3000L, Fujifilm) is added dropwise to the image sensor and spin-coated at a speed of 3000 rpm. This will form a layer acting as a green filter with a thickness around 1.96 μm on the yellow filter, effectively making them a layer of yellow-green filter.

Next, a laser patterning process is carried out by using UV pulses of a Nd:YAG laser at 266 nm (Callisto VL-C30, V Technology Co., Ltd.). This laser is used to remove alternate lines of the yellow-green filter from the pixel array, where each line is 15 μm wide. A cyclo-olefin polymer (E2110-10, Zeocoat, Zeon) was spin-coated at a rotation speed of 4000 rpm and followed by baking at 150 °C to form a thin and hard layer of surface protectant. Thereafter, a blue dye (SB-3000L, Fujifilm) is added dropwise to the image sensor and spin coated at a speed of 4000 rpm for 30 s. Next, a layer acting as blue filter with thickness around 1.56 μm is coated on the photodiodes previously coated with the yellow-green filter, as well as on the photodiodes that are not coated with a filter.

Lastly, laser patterning is carried out again with green pulses of the Nd:YAG laser at 532 nm. This green laser illuminates the photodiodes coated with the blue and yellow-green filters, and it only removes the blue filter as the yellow-green filter transmits most of the laser light. After the laser patterning process, the pixel array is coated with alternate lines of blue and yellow-green filters. Figure 3.8 summarized the fabrication process of the selective detection

layer and Figure 3.9 shows the microscope image of the selective detection layer.

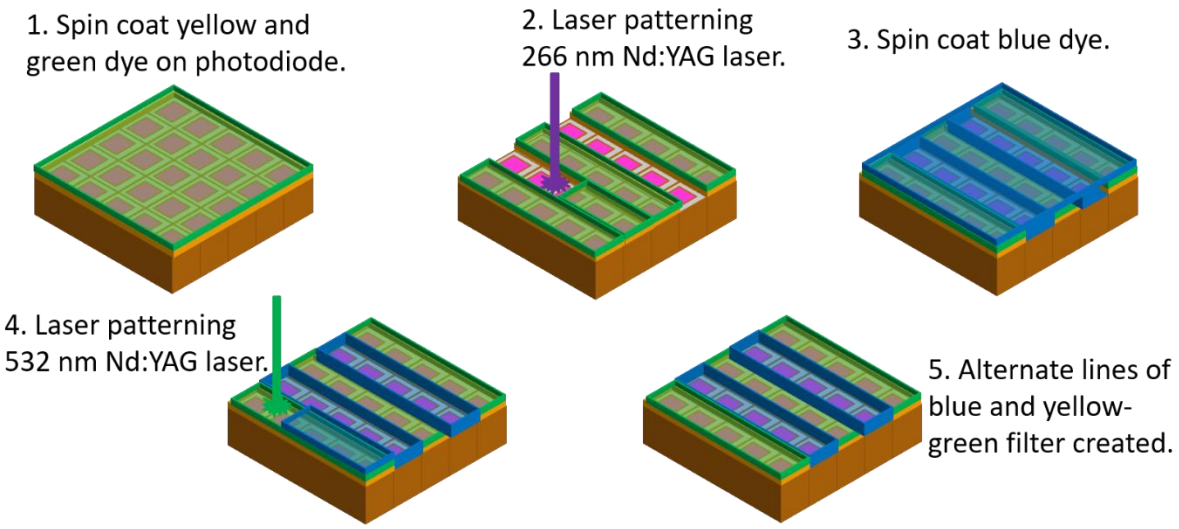

Figure 3.8: Summary of the fabrication process for selective detection layer.

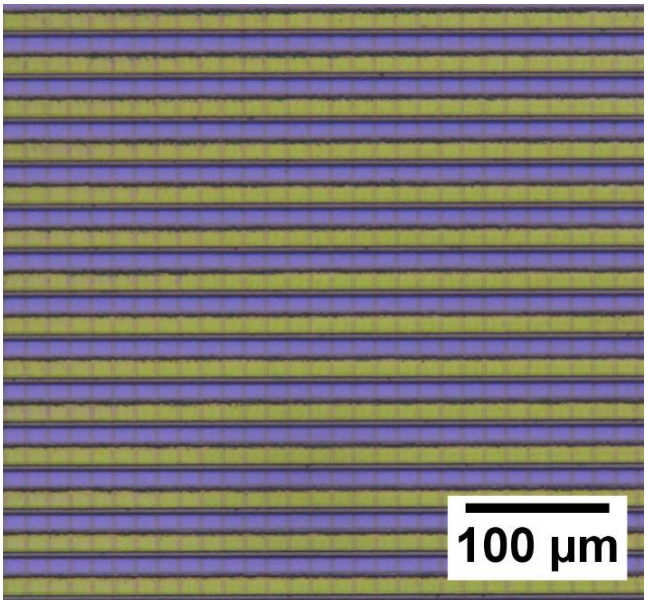

Figure 3.9: Microscope image of the selective detection layer.

3.3.2 Fabrication of the excitation light removal layer

A high-resolution FOP (J5734, Hamamatsu Photonics) is used in our design. The core pitch of this FOP is 3 μm, much finer than the pixel size. Long-pass interference filters of 460 nm wavelength and short-pass interference filters of 550 nm wavelength are coated on the FOP. This process is performed by a company (Tac Coat). After that, some pale-yellow dye solution is added dropwise on the opposite side of the short-pass filter and is spin-coated at a speed of 1000 rpm, followed by UV curing for 60 s and baking at 60 °C under vacuum for 3 h. This forms a layer acting as pale-yellow absorption filter on the opposite side of the short-pass interference filter. The aforementioned pale-yellow dye solution is prepared by mixing a pale-yellow dye powder (FDB-003, Yamada Chemical Co., Ltd.) with cyclopentanone (120-92-3, Tokyo Chemical Industrial Corporation) and optical adhesive (NOA 63, Norland Products Inc.) with a weight ratio of 1:30:30. The thickness of the pale-yellow absorption filter was found to be around 5μm.

3.3.3 Filter thickness measurement

In order to measure the thickness of a filter, the dye solution of that particular filter is prepared accordingly. Then, the dye solution is added dropwise on microscope cover glass (Matsunami Glass) and is spin-coated, illuminated with UV, and bake if needed. This will form a layer acting as that particular filter on the cover glass.

Next, the thickness of the filter casted on the cover glass is measured by using a surface profiler (Kosaka Laboratory Ltd., ET200). The surface profiler will record the difference in height between the cover glass and the filter, hence determining the thickness of the filter. For each filter, 5 measurements were taken at different side of the filter and their average was taken to obtain a more accurate measurement.

3.3.4 Assembly process

The image sensor chip is attached to a printed circuit board (PCB) using epoxy resin, and the epoxy resin is cured by heating for 10 min at 120 °C. Next, wire bonding is carried out to connect the image sensor chip to the PCB. The wire bonding area is then strengthened by covering it with epoxy resin. The epoxy resin is again cured by heating for 10 min at 120 °C. Next, the area surrounding the chip is painted with black antireflection paint (CS-37, Cannon Chemical) to prevent light from being reflected by the PCB during the experiment. Lastly, a piece of thinned high-resolution FOP with a thickness of 0.5 mm is attached to the image sensor chip by using epoxy resin to act as a protection layer. This time the epoxy resin is cured for 24 h at room temperature to avoid air bubble formation between the image sensor chip and the FOP. Weightage is applied onto the FOP to make sure it is attached properly with the image sensor chip. Then, four pieces of wire are bonded to the designated pins on the PCB so that it can be connected to the imaging interface. The excitation light removal layer is stacked on top

of the thinned FOP during the experiment. Figure 3.10 shows the summary of the assembly process while Figure 3.11(a) and 3.11(b) show photographs of the fabricated device with and without the hybrid filter respectively.

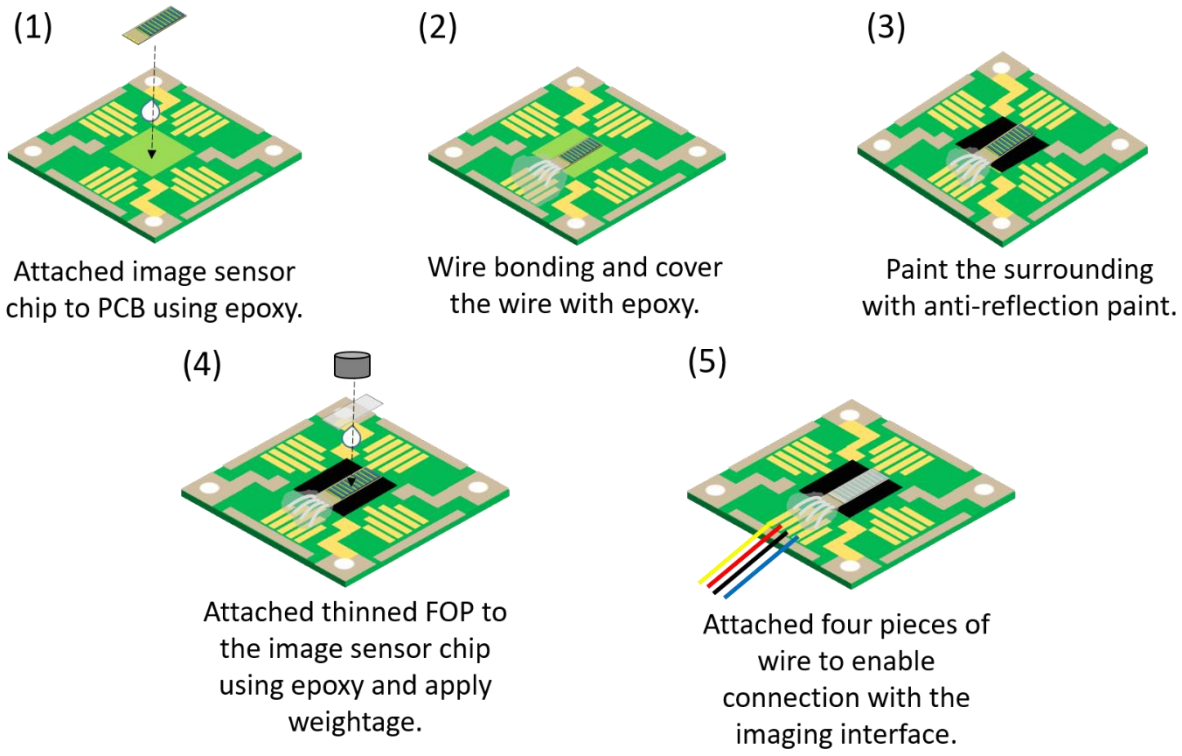

Figure 3.10: Summary of the assembly process.

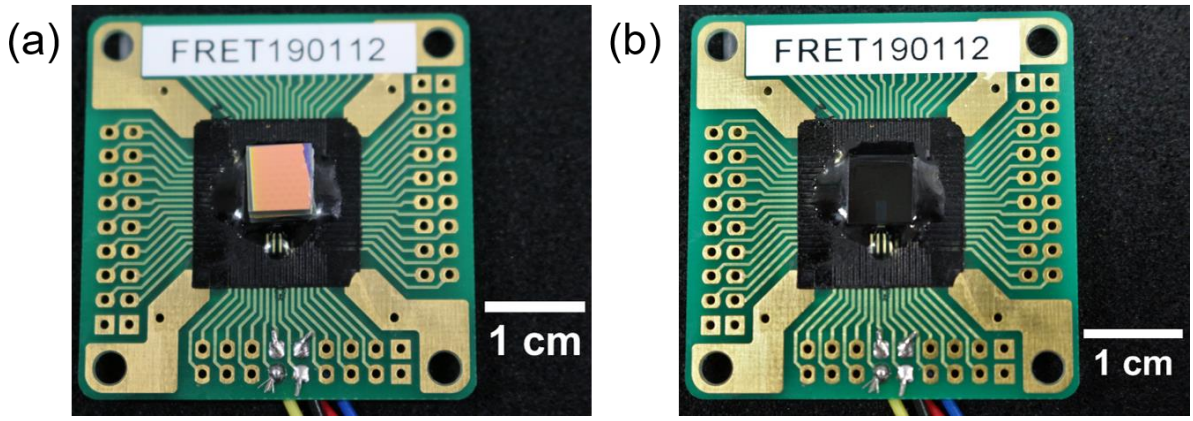

Figure 3.11(a) Photograph of the imaging device with a hybrid filter. (b) Photograph of the imaging device without a hybrid filter.

3.4 Sensor Performance

3.4.1 Excitation light extinction ratio for the excitation light removal layer

The excitation light removal layer is a hybrid filter made up of a bandpass interference filter and a pale-yellow absorption filter (FDB-003). The excitation light extinction ratio for the bandpass interference filter is essentially fixed when it is fabricated by the company, hence we can only modify the pale-yellow absorption filter to achieve the excitation light extinction ratio we desired. For fluorescence detection from CFP and YFP, an excitation light transmission less than 10^{-6} or excitation light extinction ratio less than -60 dB is preferred. This is because the quantum yield of CFP and YFP is found to be in terms of 10^{-4}. In order to detect the target fluorescence, noise level should be at least 100 times smaller than the signal intensity. Hence the excitation light transmission less than 10^{-6} is set as our target.

For an absorption filter, its light extinction ratio is directly proportional to its thickness.

However, up to a certain point, its light extinction ratio increase very slowly, even though its thickness is increased substantially. This situation is explained by Lambert's Law, where the transmittance of monochromatic light through a homogeneous, low-concentration medium becomes asymptotic when the light path length (thickness) continues to increase. In order to change the thickness of the absorption filter, the spin coating speed used to produce the absorption filter needs to be change and the thickness of the absorption filter is inversely proportional to the spin coating speed used when the dye solution's concentration is fixed.

In this case, the optimum thickness of the absorption filter should be determined to achieve a balance between the excitation light extinction ratio and thickness. For this, an experiment is carried out to determine the excitation light transmission through the excitation light removal layer with different thickness of the pale-yellow absorption filter.

In this experiment, the filters are placed on top of a power meter (Thorlabs, S130VC), and the excitation light is illuminated from the top. The excitation light is from a fluorescence microscope (Olympus, BX51WI) equipped with a mercury burner (Olympus, U-RFL-T) and an objective lens (Olympus, MPlan N 5x/0.10na). A piece of excitation filter (Thorlabs, MF434-17) is used together with the microscope to limit the central wavelength of the excitation light to 434 nm. During the experiment, another piece of excitation filter (Semrock, FF01-434/17-25) is placed directly below the objective lens to reduce the fluorescence emission from the optical system. A drawing showing the path of light of this experiment setup and the

arrangement of the samples is shown in Figure 3.12. Note that the long-pass and short-pass interference filter were coated on glass substrate, while the absorption filter (FDB-003) was casted on a microscope cover glass. The filters are added or removed when needed during the experiment. As this setup essentially eliminates most, if not all, of the unwanted fluorescence, the excitation light performance is comparable to that of a fluorescence microscope. The results of excitation light transmission through the hybrid filter are shown in Figure 3.13.

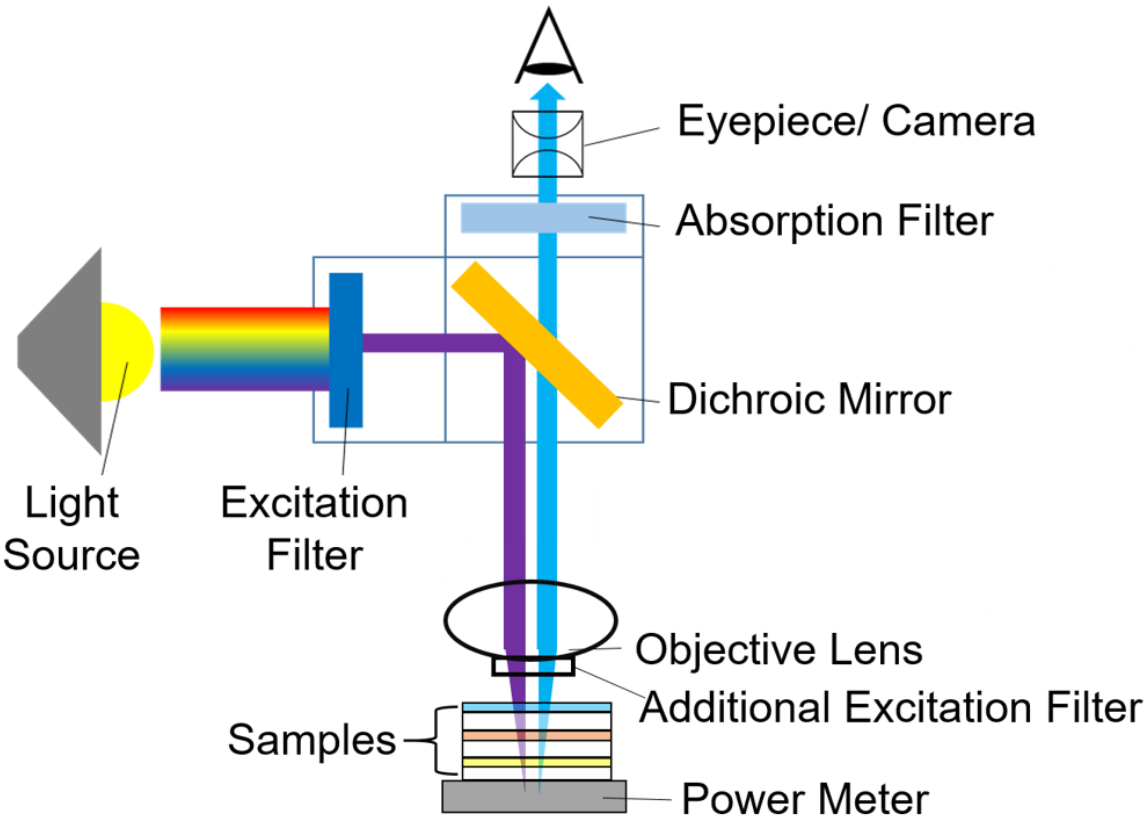

Figure 3.12: Path of light and samples arrangement of the experiment setup

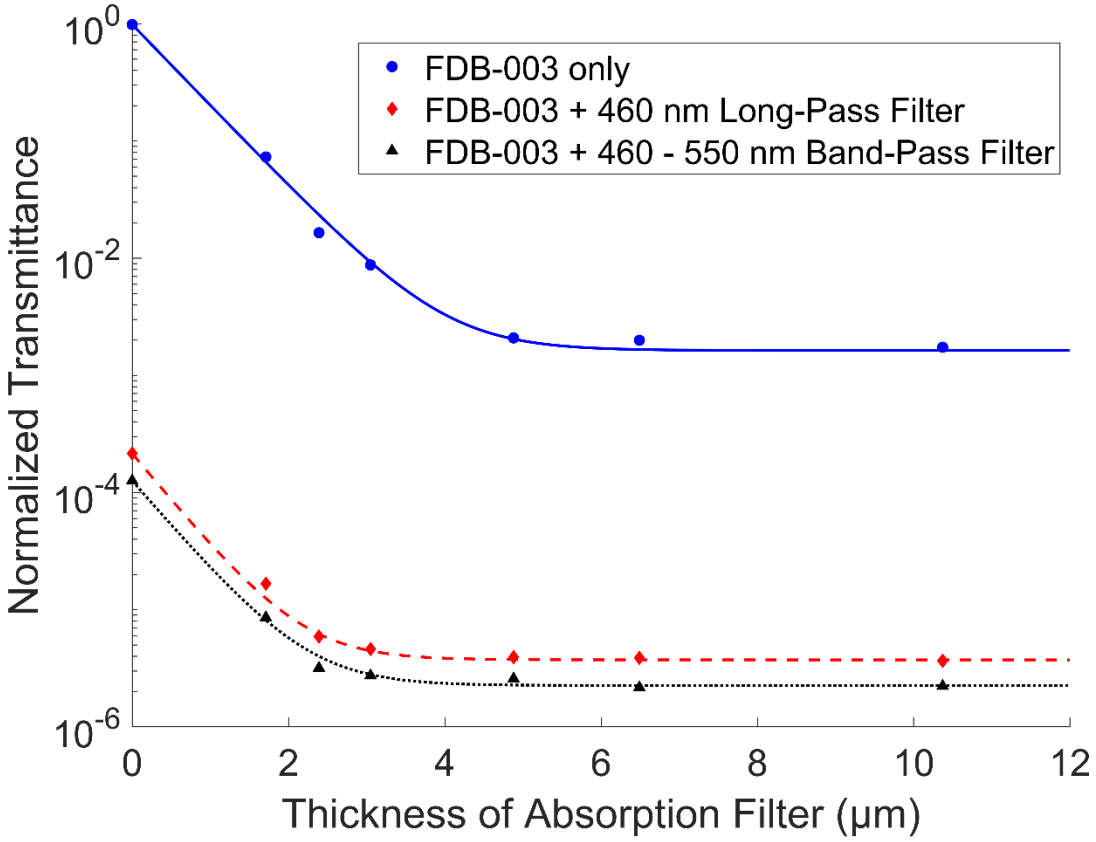

Figure 3.13: Effective transmission of excitation light the hybrid excitation removal filter. Curve fitting is carried out to fit the obtained data points to an exponential function.

From Figure 3.13, it was found that by using the absorption filter alone, the excitation light transmission is on the order of 10^{-2}. This is far from sufficient for fluorescence imaging. Moreover, when using the absorption filter alone, the absorption emits autofluorescence after absorbing the excitation light. The intensity of autofluorescence is usually greater than that of the target fluorescence of CFP or YFP from the cells and hence it is not preferable.

Next, a long-pass interference filter with a cut-on wavelength of 460 nm were added on top of the pale-yellow absorption filter to reduce the excitation light transmission and

autofluorescence. The interference filter reflects the excitation light and does not show autofluorescence. Thus, the excitation light transmission is reduced to over 10^{-5}. Although this design considerably increased the performance of the hybrid filter, the excitation light extinction capability of the hybrid filter was further improved by sandwiching a piece of 550 nm short-pass interference filter between the long-pass interference filter and the absorption filter because the FOP shows some fluorescence. Furthermore, it can transmit the cyan and yellow fluorescent light, so it will not affect the results of experiments. Lastly, it also reflects any unwanted autofluorescence with wavelength greater than 550 nm from, for example, cells, living tissues, or chambers. This further reduces the likelihood of capturing unwanted autofluorescence during the experiment. For this hybrid filter design, the excitation light transmission increases to approximately 2×10^{-6} or -57 dB if we calculate the extinction ratio instead. This excitation light extinction performance should be sufficient for fluorescence imaging.

Next, by examining the relationship between the transmission of excitation light through the filters and the thickness of the absorption filter, it was found that for all three filter designs, the excitation light transmission stopped decreasing when the thickness of the absorption filter increased beyond 5 μm. Hence, the optimum thickness of the pale-yellow absorption filter is found to be approximately 5 μm. This thickness can be achieved by spin-coating the yellow dye solution at a speed of 1000 rpm for 30 s.

3.4.2 Angle-dependent sensitivity spectrum of the full device

As the image sensor is equipped with a bandpass interference filter, the incident angle of light affects the sensitivity of the image sensor. Hence, an experiment is carried out to determine the effect of the incident angle of light on the sensitivity of the image sensor with all filters attached to it. The results of this experiment are shown in Figure 3.14.

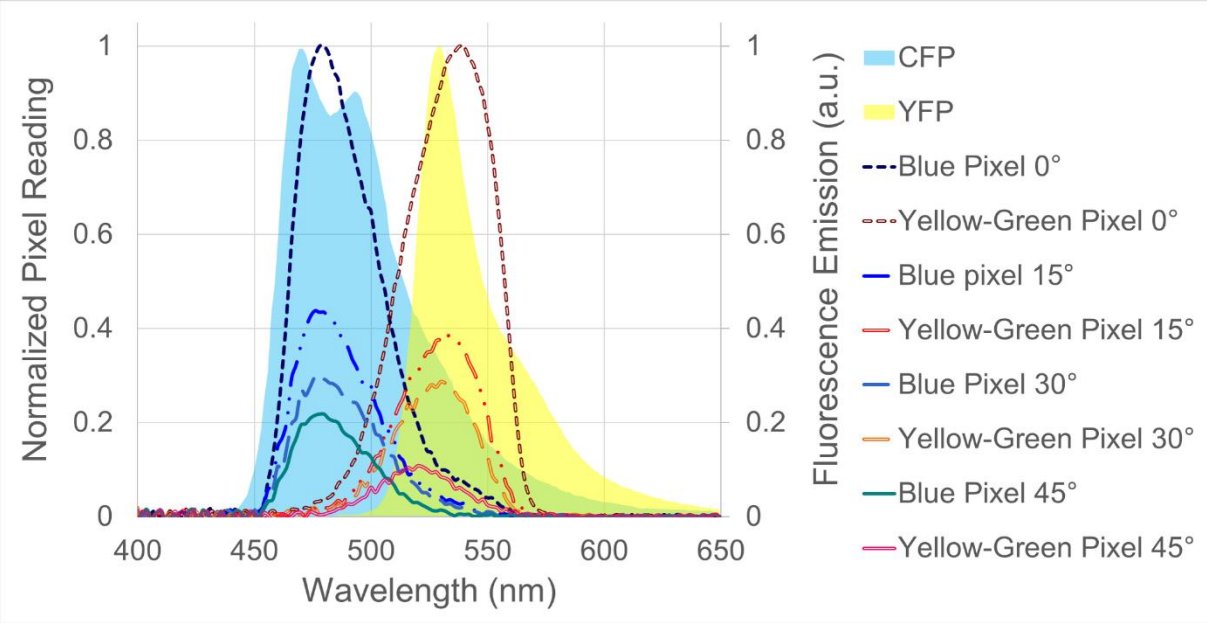

Figure 3.14: Angle-dependent sensitivity spectra of the full device

According to Figure 3.14, there is a decrease in the normalized pixel reading when the incident angle of light increases. The reduction of the normalized pixel reading is more significant for pixels coated with the yellow-green filter than for those coated with the blue filter. This is because the sensitivity of each channel is limited by two different filters. Referring to Figure 3.6, the lower limit of light transmission is limited by the absorption filter (FDB-003).

Since the transmission spectrum is shifted to a lower wavelength by tilting the incident light, the spectral shape of the blue channel is almost unaffected. In contrast, the longer-wavelength limit of light transmission for pixels coated with the yellow-green filter is determined by the short-pass interference filter. Thus, the transmission spectrum is significantly affected by the angle because of spectral shift. The sensitivity peak of the yellow-green pixel shifted by approximately 15 nm to a shorter wavelength when the incident angle of light was increased from 0 to 45°. In contrast, there were almost no changes for the peak of the normalized pixel reading spectrum of pixels coated with the blue filter when the incident angle of light was increased.

Since the target light arrives from all directions during fluorescence imaging, the image sensor will detect oblique fluorescent light with a lower intensity than the actual intensity. As the yellow-green pixels sensitivity decreases more significantly than that of the blue pixels, two neighboring pixels coated with a different filter will detect a less yellow fluorescent light than cyan fluorescent light when they arrive from the same source. As the ratio of yellow fluorescent light to cyan fluorescent light is needed to determine the FRET activity, this might cause the calculated ratio to be lower than the actual ratio. Although the performance of the image sensor decreases when the incident light is not normal, it can work very well when most of the fluorescent light is from the normal direction. However, when the fluorescent light is expected to arrive from all directions, some countermeasures can be taken. For example, the high-

resolution FOP can be replaced with a low-numerical-aperture (low-NA) FOP to reduce light with angles greater than a certain threshold, a light guide array can be used [50], or the device can be equipped with an angle-selective grating [12] to transmit normal light only.

3.4.3 Experimental results of imaging two-color fluorescent microbeads

In this experiment, the fluorescent light emitted by fluorescent microbeads of two different colors is observed using our device. Here, blue-green (F8830, Thermo Fisher Scientific) and yellow-green (F8844, Thermo Fisher Scientific) were used to provide fluorescent light. The nominal bead diameter of the blue-green and yellow-green microbeads are 10 and 15 μm respectively. On the other hand, the absorption and emission spectra of the blue-green and yellow-green microbeads are 430/465 nm and 505/515 nm respectively.

Both types of microbeads are added dropwise to a piece of microscope cover glass (Matsunami glass) with a thickness of approximately 0.05 mm and mixed. The cover glass containing the microbeads is then placed on the device after the device is set up under a fluorescence microscope. The excitation light was irradiated from above by a Hg lamp built in the fluorescence microscope (Olympus, BX51WI). The objective lens was an Olympus MPlan N 5x/0.10NA. A piece of excitation filter (Thorlabs, MF434-17) was used together with the microscope to limit the central wavelength of the excitation light to 434 nm. The fluorescence from the microbeads was captured by using both our devices as well as the fluorescence

microscope. Here, our imaging device can obtain a two-color image with a single shot, while the filter cubes must be exchanged for blue and yellow channels when using the fluorescence microscope. The microscope images serve as a reference for the image captured by our device.

Initially, the image captured by our device consists of the data in both the cyan and yellow channels. Post processing work was carried out using MATLAB (MATLAB R2018b). The cyan and yellow channel images were extracted as shown in Figure 3.15. In contrast to the microscope images, the results show that our lens-free device can detect and capture fluorescent light in the cyan and yellow color regions separately. As the pixel size of our device is 15 μm and alternate lines of blue and yellow-green filters are coated on the pixel, this causes the spatial resolution of the cyan and yellow channels of our device to be reduced to 30 μm in the vertical direction in the image. However, this spatial resolution is still sufficient for FRET imaging purposes. This is because the fluorescent proteins which being produced through genetic modification are express in cell level and the observation carried out in organ level is sufficient. Hence, high spatial resolution is not required to discriminate each individual cell and the resolution of 30 μm is sufficient for FRET imaging purposes.

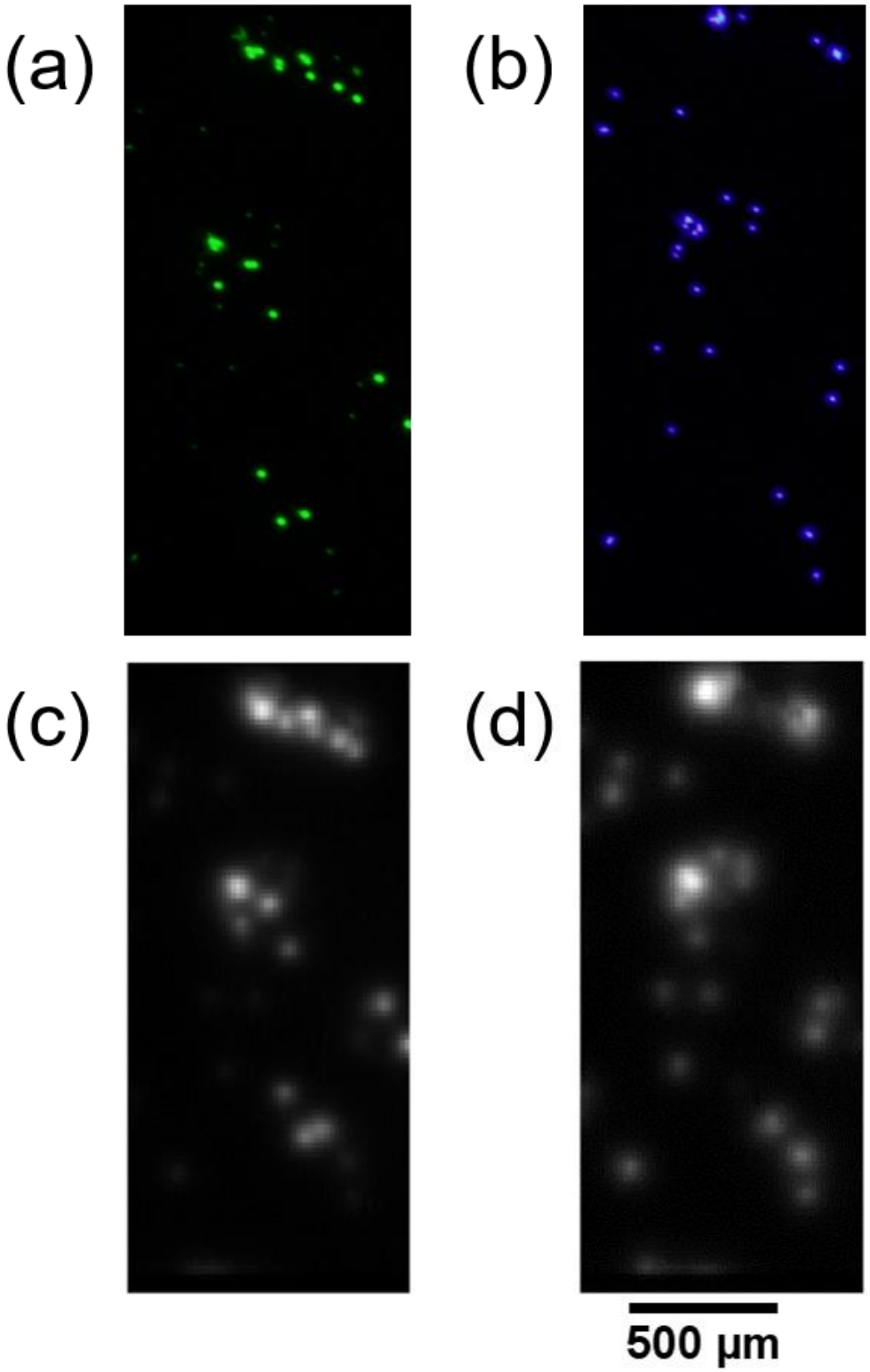

Figure 3.15 (a) Yellow channel and (b) cyan channel images captured by the fluorescence microscope. (c) Yellow channel and (d) cyan channel images captured by the lens-free device. The fluorescence microscope images show the approximate locations of the fluorescent beads, serving as a reference for the image captured by the lens-free device.

After extracting the cyan and yellow channel data, the ratio of the yellow-to-cyan channel data is obtained. To obtain a clearer ratio image, the base 10 log of the ratio of the yellow-to-cyan channel data is taken and plotted. In this image, a region with a value greater than 0 is occupied by yellow-green beads, while a region with a value smaller than 0 is occupied by blue-green beads.

Next, the cyan and yellow channel images obtained by using our device are merged and overlaid on the ratio image to give a reference for the type of microbead that occupied a certain region on the device. Figure 3.16(a) shows a base 10 log plot of the ratio of yellow-to-cyan channel data. This image indicates the color of the fluorescence. However, the intensity information is not shown. The dark area is noisy but also colored. Figure 3.16(b) shows the overlaid image obtained by combining the ratio image with the cyan and yellow channel images. In this image, both the position and the color of the beads can be verified. According to Figure 3.16, our device is capable of obtaining the ratio of yellow-to-cyan channel data and displaying it in image post processing. This is particularly important as this device will be used to study FRET activity. To determine the spatiotemporal dynamics of a pair of molecules, the FRET-to-CFP ratio is needed, and this ratio will be given by the ratio of yellow-to-cyan channel data obtained by our device. By continuously collecting all the pixel readings, i.e., “taking a movie” using the device, the changes in the ratio with time can be obtained.

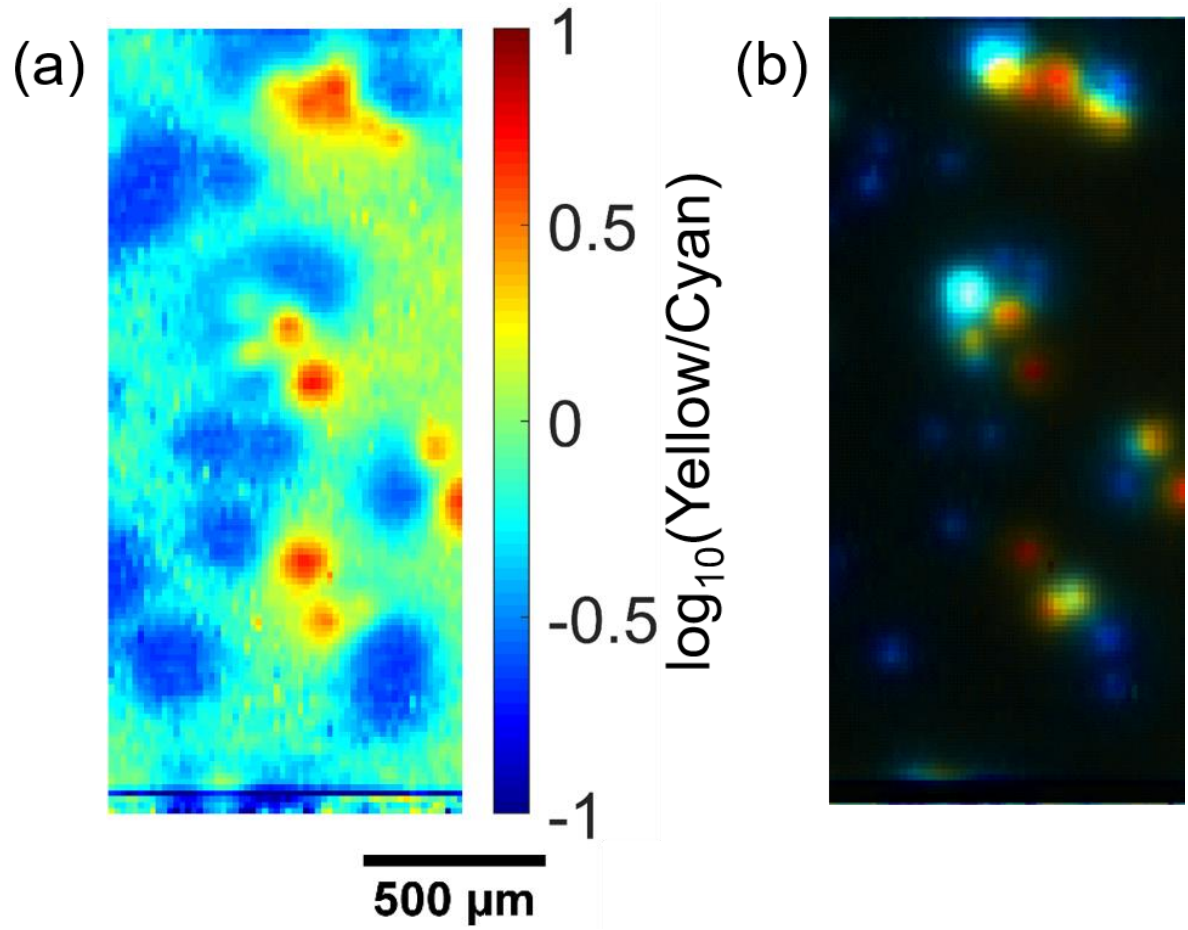

Figure 3.16: (a) Base 10 log plot of the ratio of yellow-to-cyan channel data obtained by the lens-free device. (b) Image obtained by overlaying the merged cyan and yellow channel images obtained by using our device on the ratio image.

3.5 *In vitro* FRET imaging experiment using the proposed sensor

3.5.1 Overview

In previous experiment, it had been confirmed that the sensor is capable of detecting fluorescence emitted by CFP and YFP pair. Hence, the proposed sensor is now being use in an *in vitro* FRET imaging experiment. In this experiment, the cultured cell used is consists of an EKAREV expressing HELA cell. EKAREV is an improved FRET biosensor of ERK protein

kinase, which can be used to study the ERK pathway. The ERK pathway is important in a way that it integrate external signals from the presence of mitogens such as epidermal growth factor (EGF) into signaling events that promoting cell growth in mammalian cells [28].

3.5.2 Preparation for *in vitro* FRET imaging experiment

Before the FRET imaging experiment is begin, the cell is cultured as described in [35]. Then chambers that will be used to hold the cultured cell during the FRET imaging experiment is prepared. A picture showing the chamber is shown in Figure 3.17. Next, the cultured cell is transferred to the chamber and it is rest for 1 day in order for the cell to grow at the bottom of the chamber. After that, the cultured cell in the chamber is ready to be used in *in vitro* FRET imaging experiment.

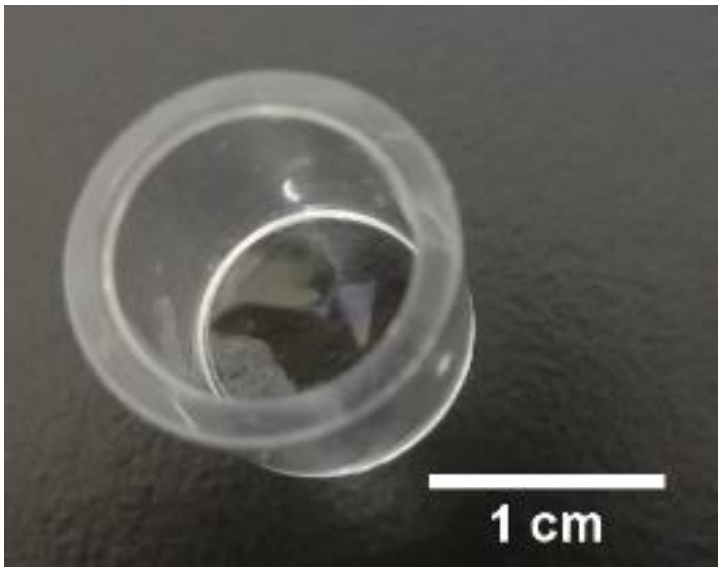

Figure 3.17: Chamber that is used to hold the cultured cell.

3.5.3 *In vitro* FRET imaging experiment

In FRET imaging experiment, the changes in FRET activity of the cultured cell is observed after EGF (a mitogen) is given during the experiment. A comparative study is also conducted where instead of EGF, cell culture media is given (no mitogen is present). The cell culture media used is DMEM^{gfp}-2 (Antibleaching live cell visualization medium DMEMgfp-2, Evrogen Joint Stock Company). Figure 3.18 illustrate the setup of the FRET experiment, while Figure 3.19 shows the photo taken after the FRET experiment. The steps to carry out the *in vitro* FRET imaging experiment is shown below.

a) The image sensor is setup under the fluorescence microscope (Olympus, BX51WI). The objective lens was an Olympus MPlan N 5x/0.10NA. Excitation light will be irradiated from above by a Hg lamp built in the fluorescence microscope.

b) A micro syringe pump (MSPE-1, AS ONE Corporation) is setup next to the image sensor so that either EGF or cell culture media can be injected into the chamber during the experiment. A syringe filled with either 1ml of EGF is setup on the micro syringe pump. Winged IV catheter (23G×5/8"(16 mm), TERUMO CORPORATION) is attached to the syringe. The needle of the catheter is slightly bended so that it can hooked to the edge of the chamber during experiment.

c) The chamber containing the cultured cell is put on top of the image sensor.

d) Excitation light is illuminated simultaneously when the image sensor is turned on. In

order to prevent photobleeching from happening too fast, periodic exposure of excitation light is carried out. In a period of 30 s, excitation light is expose for 5 s and turned off for the rest of 25s.

e) 5 minutes after the image sensor is turned on, EGF is injected into the chamber for 1 minutes in a rate of 100 µL/min. The final concentration EGF in the chamber is set to be at 50 ng/mL.

f) The imaging experiment is stopped after 30 minutes.

g) Steps c) to f) is repeated with cell culture media ($DMEM^{gfp}$-2) replacing EGF and a new chamber containing cultured cell is used.

h) Lastly, the obtained data is processed using MATLAB (MATLAB R2018b).

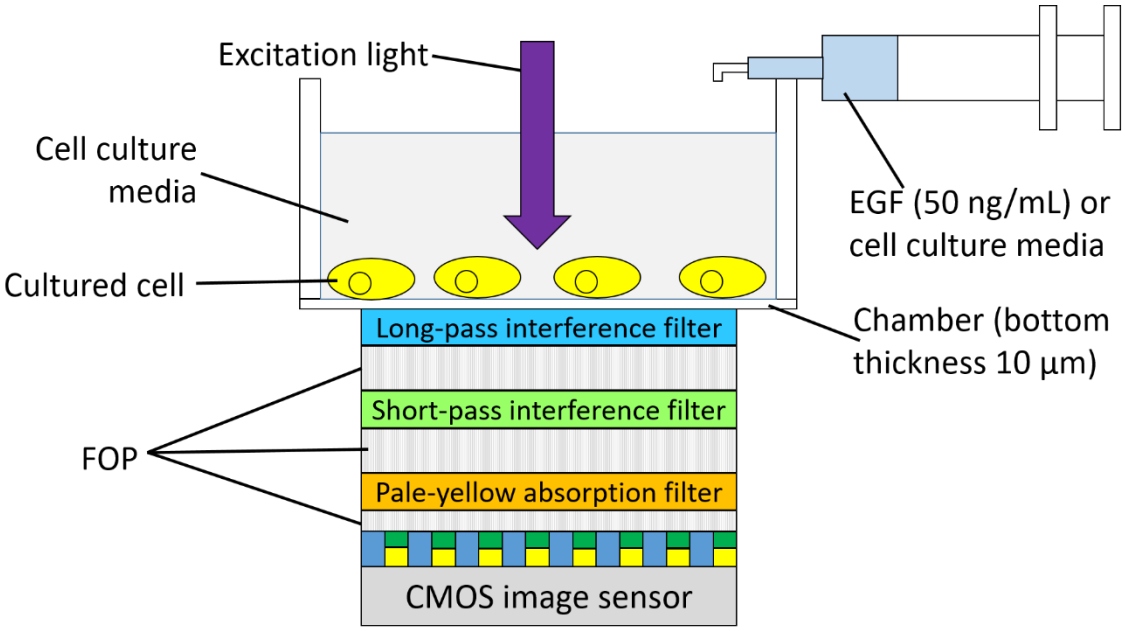

Figure 3.18: Illustration of the setup of an *in vitro* FRET imaging experiment.

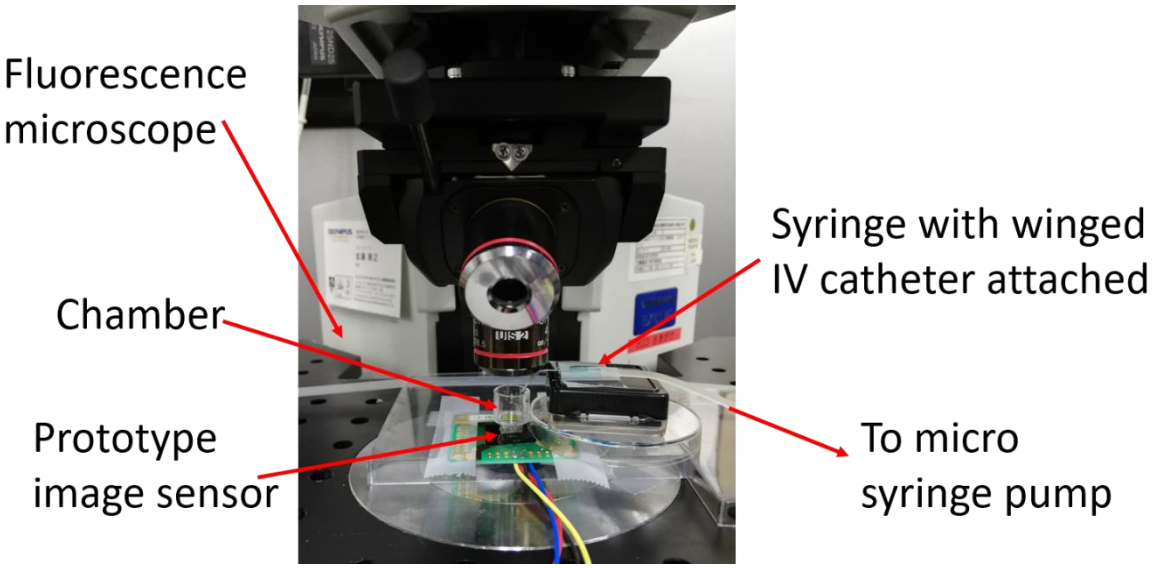

Figure 3.19: Photo showing an *in vitro* FRET imaging experiment

3.5.4 *In vitro* FRET imaging experiment results

Figure 3.20(a) shows the results of FRET imaging experiment where EGF is injected 5 minutes after the image sensor is turned on. Figure 3.20(b) on the other hand, shows the control experiment where cell cultured media is injected 5 minutes after the image sensor is turned on. In this set of experiment, pulsed excitation light was used. The period of the excitation light is 30 s, where the first 5 s is the on time of the excitation light while the remaining 25 s is the off time of the excitation light. Here, the FRET activity is given by the ratio of yellow fluorescent light intensity to cyan fluorescent light intensity (hereafter known as YFP/CFP ratio) collected by the image sensor. According to figure 3.20(a), it is obvious that there is an increase in YFP/CFP ratio after EGF is given. On the other hand, there is no significant changes in the YFP/CFP ratio where cell cultured media is given after 5 minutes in the control experiment. This results agree well with previous studies where the introduction of EGF will cause changes

in the internal structure of the cell in which it will boost the FRET activity of the cultured cell [28]. This results also confirm the capability of the proposed image sensor to detect the changes in FRET activity in an *in vitro* FRET experiment.

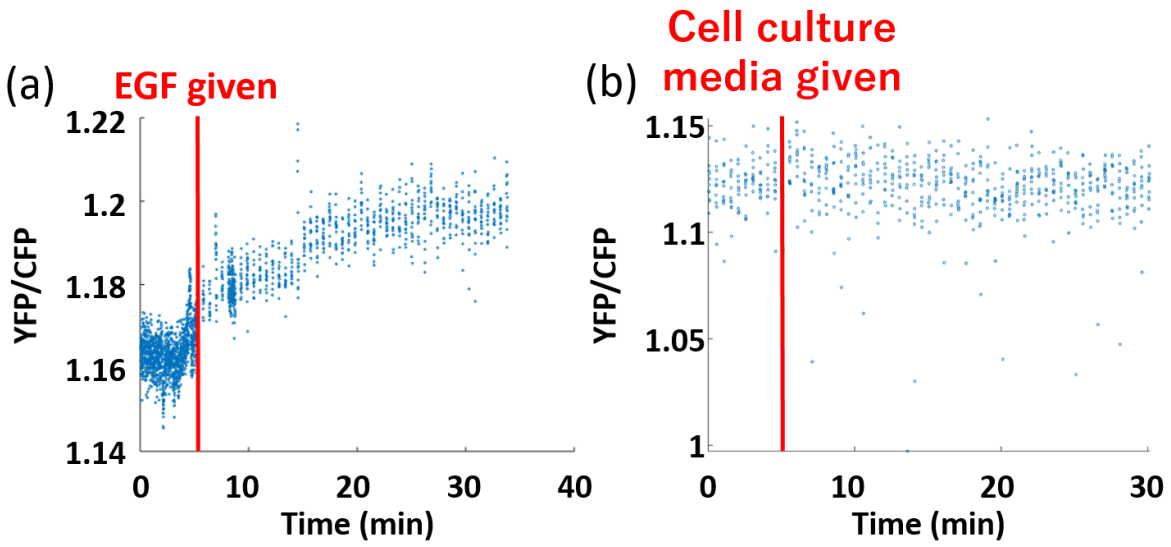

Figure 3.20: *In vitro* FRET imaging experiment results where (a) EGF and (b) cell culture media was injected 5 minutes after the experiment started.

For FRET imaging experiment, observation carried out in terms of minutes is normally sufficient. However, the sampling rate of the image sensor is much faster, normally in terms of seconds. This allow us to average the data points and increase the signal-to-noise ratio.

In the *in vitro* FRET experiment, a chamber will be used to hold the cultured cell during the experiment. In this way, we assume all the cells will "stick" to the bottom of the chamber. However, in actual scenario, this might not be the case. There might be a chance where a minimal amount of cell will end up floating in the cell culture media. This probably due to

improper preparation and handling process when the cultured cell is being transfer from a petri dish to the chamber. The fluorescence emitted by the floating cells might or might not be detected by the image sensor. This is depending on a few parameters, for example the distance between the floating cell and the image sensor, the scattering coefficient of the cell culture media, and the emission intensity of the floating cell. However, since the amount of floating cell is very low, the fluorescence contributed by these cells can be ignored since it will not significantly alter the results obtained.

Next, ratiometry is being used to present the result of FRET experiment instead of individual changes of cyan and yellow fluorescence in order to lower the contribution of noises in the data. This is because the pixel will detect some noise in the form of the counterpart fluorescence. For example, the pixel coated with blue filter will detect a low amount of yellow fluorescence and vice versa. By using ratiometry instead, the contribution from these noises can be neglected as their contribution will be cancel out instead.

3.6 Outlook for *in vivo* FRET imaging using the proposed sensor

As the *in vitro* FRET imaging experiment is successfully carried out, the attention will now be shifted towards *in vivo* FRET imaging experiment in order to test the fluorescence detection performance of the proposed image sensor on living animal. Other than the fluorescence detection performance, the lifetime of the image sensor after it is being implanted into the body

of a lab animal need to be determine as well. This is because the final goal of this research is to develop an image sensor that can be used to carry out long term *in vivo* FRET imaging on freely moving animal. Hence the lifetime of the sensor must be greater than the expected period of the experiment.

In order to implant the image sensor into the body of a lab animal, the image sensor must be made waterproof and bio-compatible. This can be done by coating the image sensor with a layer of parylene-C. Till date, after 6 months, the image sensor implanted into a mouse brain is still functioning properly. However, in some cases, a clear image cannot be obtained using the image sensor even though it is still working properly after the implantation work. This is because some tissue is regenerated near the image sensor after the implantation and this tissue will block some part of the image sensing region and obstruct the image acquisition work. However, this situation can be improved by appointing highly skilled personnel to carry out the implantation work. Hence, the lifetime of image sensor implanted into the body of lab animal should be long enough for long-term *in vivo* FRET imaging experiment.

Chapter 4

Wireless module for *in vivo* imaging

4.1 Overview

The implantable image sensor is designed with minimum functions. Thus, its size and weight are very small and light. However, it has wires to connect it to a control system. The presence of wires bring forth some problems and they remain as one of the most important issues to be solved before realizing long-term *in vivo* imaging. For example, wired connected system often restrict the movements of host animals. Moreover, some animals tend to remove the wires and connecters on their body through scratching and biting during experiment. This might cause data loss and additional cost is needed to replace the broken wires and connectors. Besides, tangling of wires also often occurred due to moving and rotation of the animal body. Although it is possible to introduce a commutator to the system to prevent tangling, however the additional part will introduce additional noise to the system and degrade the signal quality. Lastly, single channel imaging no longer satisfy the research needs nowadays. Most of the imaging systems has gone to multi-channel imaging. This means that more wires will be added to the system and this is not favorable. Although multiplexing system can limit the increase in the number of wires present, it still cannot remove all of the wires [51]. In order to solve this issue, it is required to make the system wireless. In this chapter, a wireless system was developed by using Bluetooth protocol that is widely used in electronic devices.

4.2 Wireless *in vivo* imaging system

Wireless communication technology has been widely prevailed and implemented in various devices such as PCs and smartphones. In particular, Wi-Fi (IEEE 802.11), which is used as a wireless LAN, and Bluetooth (IEEE 802.15.1) are widely used. Since high performance and functions can be used relatively easily, it is consider to adopt these widely spread standards in this study.

Generally, for *in vivo* imaging, small animal such as mouse will be used. The weight of an adult mouse is around 20 g - 30 g. Therefore, even if the device is placed on the back, the allowable weight is considered to be about several grams. Although the weight of image sensor itself is around 1 mg, which is sufficiently lightweight. However, a peripheral circuit, a wireless communication module, and a power supply like a battery are required to form a complete wireless imaging system.

As a stable power supply element, a coin-shaped small battery can be used. In particular, lithium primary batteries have an output voltage of 3 V, and one battery can drive a standard CMOS circuit. There are various sizes depending on the application, but there is the above-mentioned weight limitation for mounting the device on a mouse, which is about 2 g at most.

For *in-vivo* imaging, it is necessary to keep operating with a battery for at least one sequence of experiments, approximately 12 hours of continuous operation. The experiment assumed in this study is the observation of a changing phenomenon in several minutes to several tens of

minutes. Thus, high-speed imaging capability is not required. In addition, with regard to spatial resolution, it is assumed that probe proteins by genetic manipulation are expressed in cells, and observation at the organ level is enough. Therefore, it does not require high resolution to discriminate individual cells. Thus, a relatively low communication speed is sufficient, and a wireless communication technique with low power consumption is suitable for our purpose.

From the above conditions, a wireless communication device based on the Bluetooth Low Energy (4.0) was developed. Although it has a low effective communication speed of about 10 kbps, it consume less power compared to typical high speed wireless device.

The configuration of the proposed system is shown in Figure 4.1. The image sensor is implanted in the body, and a device equipped with a microcontroller and a wireless communication module for controlling it is placed on the back. This is remotely controlled from the PC, and data from the image sensor is sent to the PC and stored.

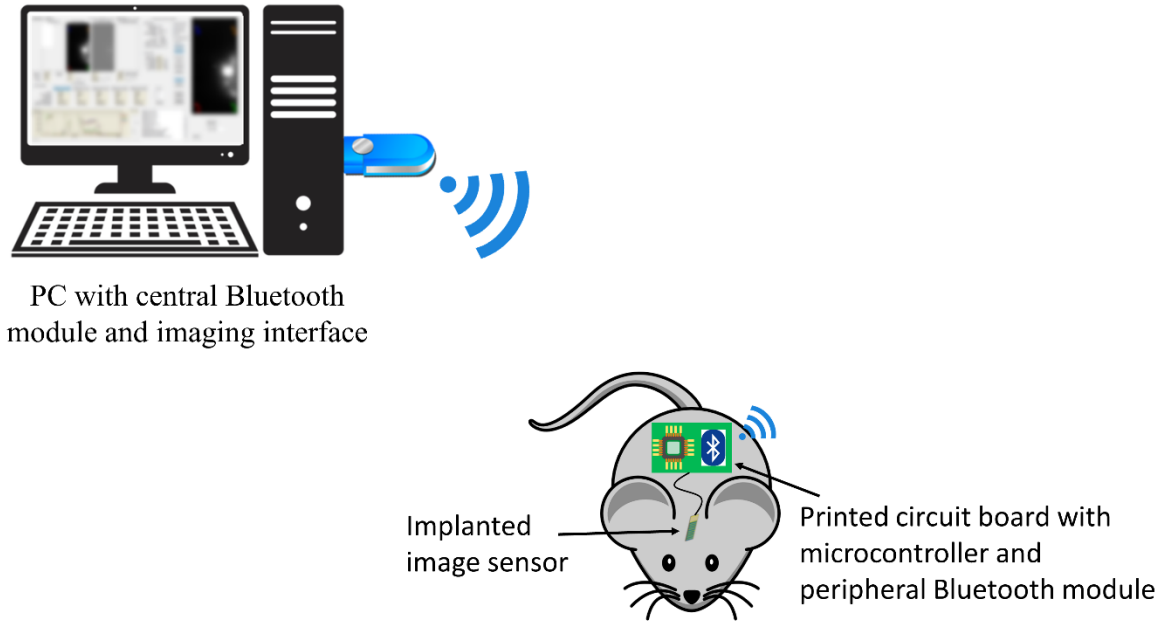

Figure 4.1: General concept of the wireless module

4.3 Design of the prototype wireless device

Figure 4.2 shows the block diagram of the prototype wireless *in vivo* imaging device. The purpose of this module is to achieve the wireless transfer of image data obtained by our CMOS image sensor.

The image sensor requires a control clock signal for operation, and the output is an analog voltage signal. These signals cannot be handled directly by the bluetooth module (ZEAL-LE0, ADC Technology Inc.). Therefore, a microcontroller (PIC 16F1704, Microchip) was adopted. The microcontroller performs serial communication between Bluetooth by UART, which is a kind of serial communication protocol. After the power is turned on, the microcontroller enters a standby state, and when it receives an image acquisition start signal, it outputs a control CLK

signal to the image sensor. In the image sensor, the selected pixel is sequentially moved by the CLK signal, and an analog voltage corresponding to the amount of light read by the pixel is output. The microcontroller receives this signal and converts it to a digital signal by the internal ADC. The ADC has 10-bit resolution, but is rounded to 8 bits and transmitted to reduce the amount of data. Also, in the prototype device, an image sensor of 120×268 pixels was used, but the number of pixels per frame was reduced to 16×30 by skipping rows and columns. Although simple data reduction was performed in this study, it is also possible to perform averaging or imaging only a specific area by data processing on a microcontroller. Digitized image data is transferred to the BLE module in serial communication by the UART and then transmitted to the PC by the BLE module. The whole prototype system is powered up by using two pieces of 1.5 V AA battery. Figure 4.3 shows the photo of the wireless module.

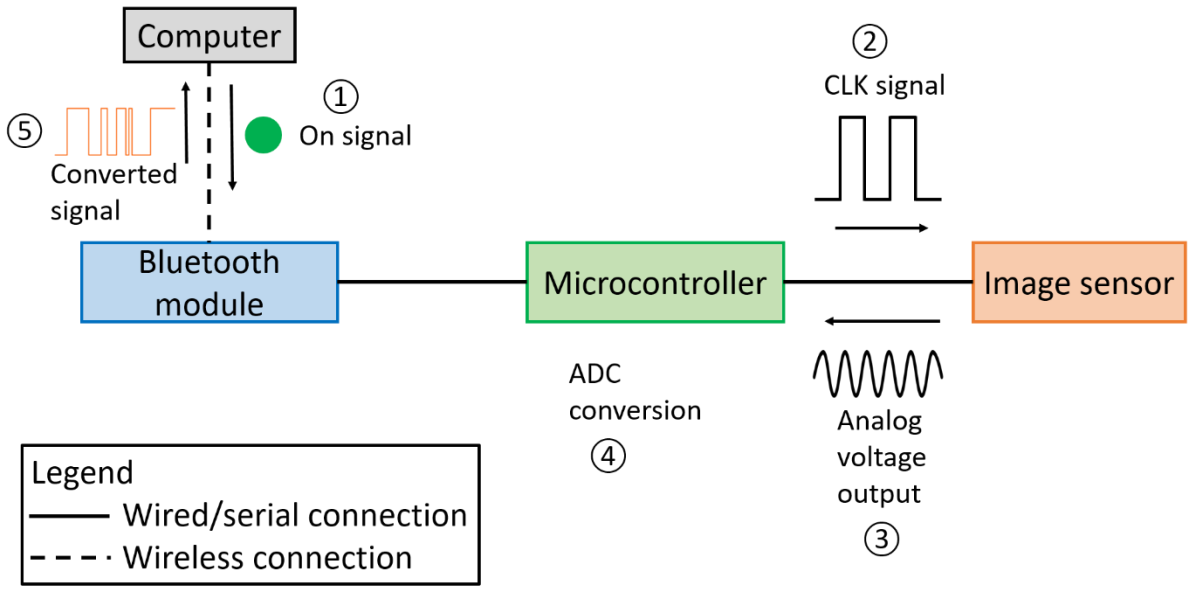

Figure 4.2: Block diagram showing the working principle of the prototype wireless device.

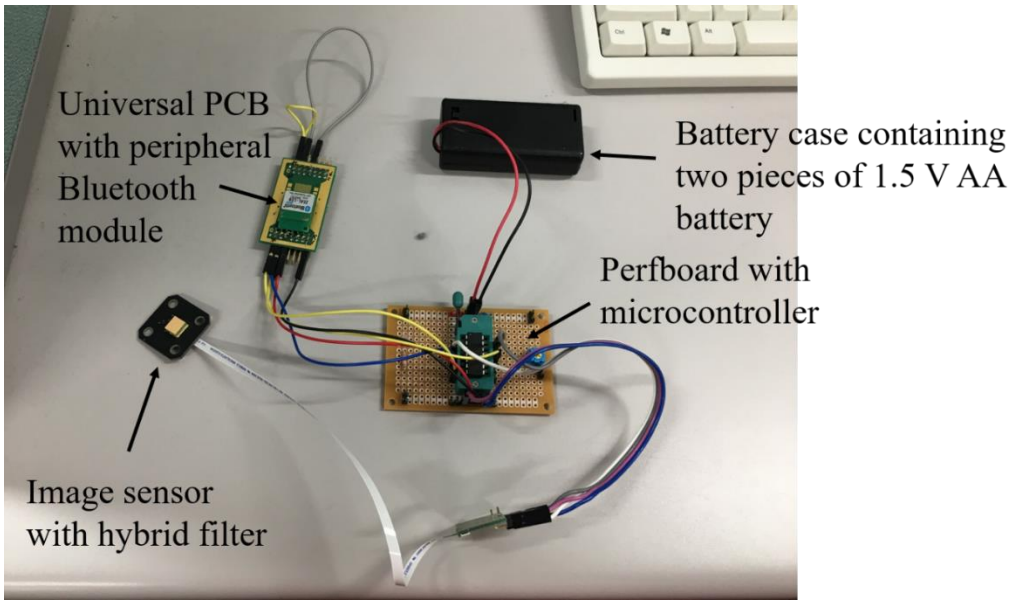

Figure 4.3: Photo of the prototype wireless module

4.4 Imaging software

The imaging software was developed for wireless imaging system. This software is modified from the software for wired USB imaging. It is coded in Visual C++ and Microsoft visual studio was used for development. The screen of the software is shown in Figure 4.4.

The Bluetooth module is recognized as a virtual COM port. Thus, it can be deal with conventional serial communication. Some settings are optimized to the present Bluetooth module. In order to keep a stable connection, the communication speed was set to 9600 bps.

In the figure, the target on which the letters of NAIST was contact imaged as an imaging example. In the red rectangle in Figure 4.4, it can be seen that the first four characters were successfully imaged. The frame rate was 1.7 fps for an image of 16 × 30 pixels, which is slower

than a typical video rate. However, it is estimated that FRET / BRET imaging which changes in a span of several minutes to several tens of minutes is sufficiently applicable.

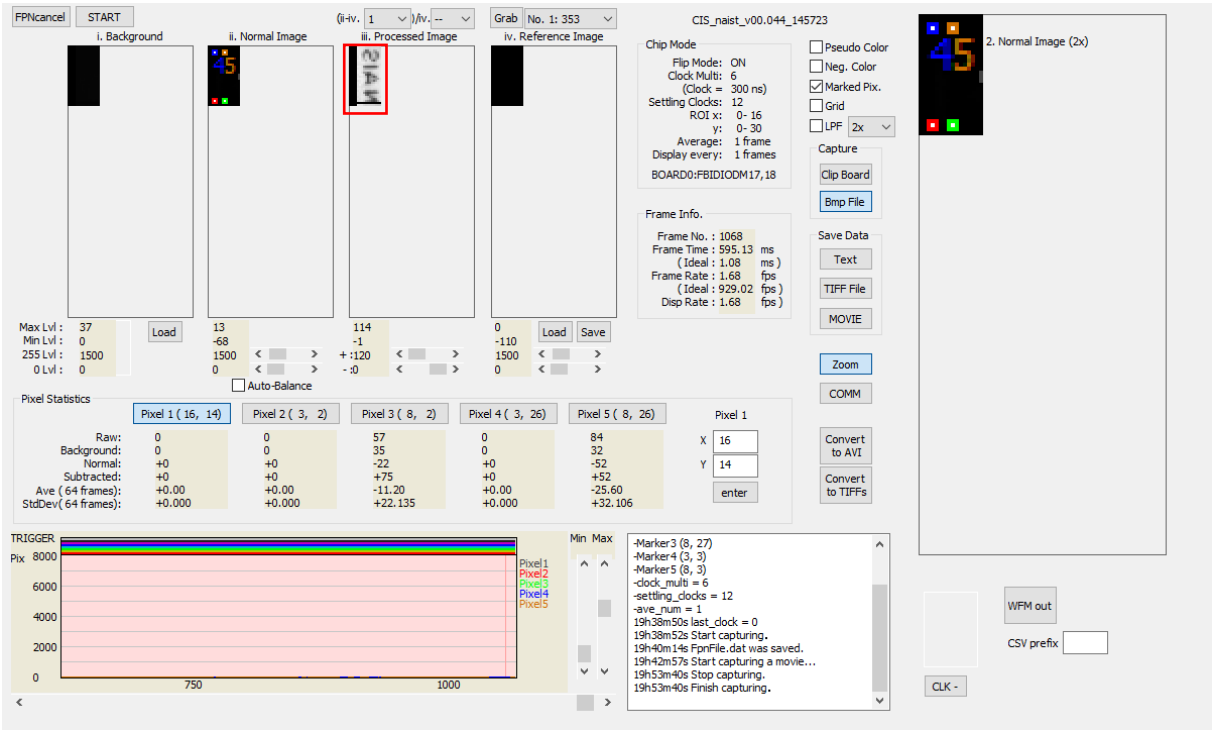

Figure 4.4: Imaging software used for wireless imaging and data storage.

4.5 Perspective for small wireless *in-vivo* imaging device

The prototype system shown in the previous section was developed to confirm basic operation of wireless image transfer. Thus, it was too large and heavy to put on a mouse. From the previous work, the weight of the implantable image sensor is approximately 0.02g or less [52]. This means that the sensor is sufficiently light even for mice. The microcontroller was in a DIP package. This is because it can be easily rewrite by using a writing system with a zero-insertion-loss socket. By replacing it with the same chip with a small surface mount package, it can be further miniaturized. For example, a package of QFN-20 has dimensions of 4.0 mm

× 4.0 mm × 0.9 mm and a weight of approximately 50 mg.

Due to high demand for IoT device applications, small Bluetooth modules have been developed. For example, a module integrated with an antenna as light as 35 mg is commercially available. Also, the weight of the circuit board can be reduced by designing a custom PCB.

It is expected the battery would be the heaviest component in the wireless imaging device. The weight of a small coin shaped battery is around 1 g, hence making the total weight of the device to be around 2-3 g. This value is acceptable for small animals like mice. However, the problem of the proposed device should be coming from the limited battery capacity. By reducing power consumption of the image sensor and data transfer rate, operation time longer than several hours could be realized.

4.6 Comparison with other image sensing system

In this section, a comparison had been made to compare the performance of our image sensor with other image sensor reported previously. Table 4.1 shows the performance summary of our image sensor and its comparison with other sensors reported recently.

Table 4.1: Performance summary and comparison with other sensors

Parameter	Khiarak *et al.* [53]	Henderson *et al.* [54]	Sasagawa *et al.* [11]	This work
Process (μm)	0.18	0.040	0.35	0.35
Supply voltage (V)	1.8	1.5	3.3	3.3
Pixel array size	1	192 × 128	120 × 268	60 × 134
Pixel size (μm^2)	200 × 200	18.4 × 9.2	7.5 × 7.5	15 × 15*
Fill factor (%)	-	41	44	61
Dynamic range (dB)	86	-	60	60
Sampling frequency (fps)	20 k	18.6 k	2	1.7
Observation target	Green fluorescence	Photon	Green fluorescence	Cyan and yellow fluorescence (FRET)
Wireless	Yes	No	No	Yes
Wireless transfer rate (bps)	115200	-	-	9600

*Spatial resolution reduced to 30 μm when yellow-to-cyan channel ratio is being calculated

From Table 4.1, it was found that our image sensor is the only image sensor reported that can be applied in FRET imaging, where the simultaneous detection of two different fluorescence is required. Among the compared imaging system, our system is one of the system with wireless function enable on it, while the other one being [53]. This is because both system aimed to apply the imaging system to study on freely moving animal. Next, our image sensor have the slowest sampling frequency and one of the largest pixel size. This is due to the nature of FRET experiment. Since the changes in FRET activity normally happened in terms of minutes, the low sampling rate will not post any problem on data acquisition on the experiment.

In fact, the data amount is more than sufficient that multiple frame obtained by the image sensor can be averaged to further reduce the noise and enhance the signal-to-noise ratio. Next, as the fluorescence emitted during the FRET experiment are coming from fluorescent proteins, which produced through bio-engineering processes, it will be expressed in cell level. In FRET imaging experiment, observation is carried out in organ level to study the interaction between various target in the organ. Hence, high spatial resolution is not need as we do not need to discriminate each individual cell and the spatial resolution of 30 μm is more than sufficient for FRET imaging purpose.

The downside of our image sensor lies with its dynamic range. It has a dynamic range of 60 dB, which is the same as the image sensor reported in [11], which is also produced by our group for green fluorescence imaging. However, the image sensor still capable to detect the target fluorescence thanks to the high performance hybrid filter equipped on it which enable it to largely cut down excitation light. However, the image sensor chip can be redesign in the future to improve its dynamic range and increase its fluorescence detection capability. This comparison also shows that even though our image sensor is not state-of-the-art type, but it is still the first application in FRET imaging and its performance suit the needs for FRET imaging. Moreover, our image sensor also has slower wireless data transfer rate compared to other. However, since this device is made specially for FRET imaging purpose, this rate is enough to archive its purpose.

Chapter 5

Summary

The main purpose of this thesis is development of an implantable CMOS image sensor that can be used for FRET imaging in order to visualize activities of molecules in the body. The image sensors used in this research were basically the same as previous works [19, 38]. In this work, a high performance filter suitable for the sensor was newly developed in order to block excitation light and simultaneously transmit two different fluorescent light. Dual-color fluorescence image acquisition with image sensor equipped with this filter was demonstrated.

The implantable sensor has a lens-free structure and contact imaging is performed because it is very small. However, it is difficult to achieve high excitation rejection ratio by an interference filter, which is usually used as an emission filter in fluorescent microscopy. In order to solve this problem, a hybrid emission filter was developed. FRET imaging requires to distinguish two-color fluorescence from CFP and YFP. Thus, fabrication process to apply a two-color filter array on a chip was established. The image sensor with such design can perform well in FRET imaging experiment and it should be the first application of lens-free imager in FRET imaging.

Also, a wireless system was developed for long-term *in vivo* imaging. Previous implantable image sensors were very small and light weight, but connected to external equipment with wires. Thus, the behavior of the observation target such as a mouse was limited. In this study, a wireless communication module based on Bluetooth low energy was adopted to build a wireless

system. The prototype successfully transmitted images obtained by the sensor although the system was too large and heavy to put on a mouse for *in-vivo* imaging. It is expected that the system will be shrunk by redesigning with miniaturized components.

5.1 Conclusion of this work

From Chapter 3, lens-free dual-color fluorescence imaging device was developed. The target fluorophores are CFP and YFP. In FRET imaging, only the CFP is excited. The filter to detect these fluorescence is composed of an emission filter for excitation light rejection and two-color filter array to separate cyan and yellow fluorescence.

The emission filter has a hybrid structure of an interference filter and an absorption filter. These filters cover their shortcomings complementary. In order to stack these filter without decreasing spatial resolution, fiber optic plates were used. The developed emission filter shows excitation light transmittance of approximately 2×10^{-6}. This performance would be acceptable for fluorescence imaging of fluorescent proteins such as CFP and YFP.

In the conventional image sensor, color resist is used for color filters on a pixel array because the color pixel pattern can be fabricated by photo lithography. However, high performance wavelength separation is required in FRET imaging. Especially, color resist for YFP fluorescence are not available. In this study, we used a polymer film doped with yellow dye suitable for YFP fluorescence detection. A laser ablation method was used for patterning.

By using this technique, two-color pixel array for CFP and YFP fluorescence was successfully fabricated.

From Chapter 4, a prototype of wireless imaging system was developed. The imaging device was built by using a Bluetooth module and a microcontroller integrated with an analog-to-digital converter. This system has many common components with our wired implantable sensor system. Thus, the imaging software was developed with a little modification from the wired system version. The wireless transfer of 16×30-pixel image at a frame rate of 1.7 fps was demonstrated. The transfer speed was much lower than the wired system. However, it is acceptable for imaging of molecule activity based on FRET.

5.2 Future outlook

In this study, an image sensor for two-color fluorescent imaging has been developed. In the next step, *in vitro* imaging of cultured cell expressing FRET biosensors should be performed in order to demonstrate the performance of fluorescence detection in living animal.

Next, redesigning of the image sensor chip needs to be carried out in order to improve its sensitivity. This is because the fluorescence emission of CFP and YFP are very low. Although the current image sensor chip have sufficient dynamic range to detect these fluorescence, the performance of the sensor can be further improve by increasing its dynamic range. This can be done by redesigning the photodiodes on the image sensor to increase the fill factor of the

photodiodes. In this way, the light sensing region on the photodiode increases and it will be much sensitive to the target fluorescence.

Also, the wireless imaging system must be shrunk to apply for *in vivo* imaging experiment. This can be realized by designing a PCB board and using the components with small packages. By combining these techniques, long-term *in-vivo* imaging would be achieved. It is expected that the system can contribute to new findings in biology and biomedical fields. For example, research aimed to understanding cancer development will largely benefited from this system. This is because a major obstacle on such research is that a long-term *in vivo* FRET imaging cannot be conducted on freely moving animal up to this point due to instrument limitations. By utilizing this system, major breakthrough in understanding cancer development can be expected and further development in such research can even leads to the development of cancer reversing mechanism, as well as more effective drugs for cancer treatment.

References

1. Seo, S., T.-W. Su, D.K. Tseng, A. Erlinger, and A. Ozcan, *Lensfree holographic imaging for on-chip cytometry and diagnostics.* Lab on a Chip, 2009. **9**(6): p. 777-787.
2. Bishara, W., T.-W. Su, A.F. Coskun, and A. Ozcan, *Lensfree on-chip microscopy over a wide field-of-view using pixel super-resolution.* Optics express, 2010. **18**(11): p. 11181-11191.
3. Zheng, G., S.A. Lee, Y. Antebi, M.B. Elowitz, and C. Yang, *The ePetri dish, an on-chip cell imaging platform based on subpixel perspective sweeping microscopy (SPSM).* Proceedings of the National Academy of Sciences, 2011. **108**(41): p. 16889-16894.
4. Pang, S., C. Han, M. Kato, P.W. Sternberg, and C. Yang, *Wide and scalable field-of-view Talbot-grid-based fluorescence microscopy.* Optics letters, 2012. **37**(23): p. 5018-5020.
5. Göröcs, Z. and A. Ozcan, *On-chip biomedical imaging.* IEEE reviews in biomedical engineering, 2013. **6**: p. 29-46.
6. Han, C., S. Pang, D.V. Bower, P. Yiu, and C. Yang, *Wide field-of-view on-chip Talbot fluorescence microscopy for longitudinal cell culture monitoring from within the incubator.* Analytical chemistry, 2013. **85**(4): p. 2356-2360.
7. Lee, S.A., X. Ou, J.E. Lee, and C. Yang, *Chip-scale fluorescence microscope based on a silo-filter complementary metal-oxide semiconductor image sensor.* Optics letters, 2013. **38**(11): p. 1817-1819.
8. Jin, D., D. Wong, J. Li, Z. Luo, Y. Guo, B. Liu, Q. Wu, C.-M. Ho, and P. Fei, *Compact wireless microscope for in-situ time course study of large scale cell dynamics within an incubator.* Scientific reports, 2015. **5**: p. 18483.
9. Ozcan, A. and E. McLeod, *Lensless imaging and sensing.* Annual review of biomedical engineering, 2016. **18**: p. 77-102.
10. Takehara, H., O. Kazutaka, M. Haruta, T. Noda, K. Sasagawa, T. Tokuda, and J. Ohta, *On-chip cell analysis platform: Implementation of contact fluorescence microscopy in microfluidic chips.* Aip Advances, 2017. **7**(9): p. 095213.
11. Sasagawa, K., A. Kimura, M. Haruta, T. Noda, T. Tokuda, and J. Ohta, *Highly sensitive lens-free fluorescence imaging device enabled by a complementary combination of interference and absorption filters.* Biomedical optics express, 2018. **9**(9): p. 4329-4344.
12. Papageorgiou, E.P., H. Zhang, S. Giverts, C. Park, B.E. Boser, and M. Anwar, *Real-time cancer detection with an integrated lensless fluorescence contact imager.* Biomedical optics express, 2018. **9**(8): p. 3607-3623.
13. Roy, M., D. Seo, S. Oh, J.-W. Yang, and S. Seo, *A review of recent progress in lens-free imaging and sensing.* Biosensors and Bioelectronics, 2017. **88**: p. 130-143.

14. Greenbaum, A., W. Luo, T.-W. Su, Z. Göröcs, L. Xue, S.O. Isikman, A.F. Coskun, O. Mudanyali, and A. Ozcan, *Imaging without lenses: achievements and remaining challenges of wide-field on-chip microscopy.* Nature methods, 2012. **9**(9): p. 889.
15. Masters, B.R., *The development of fluorescence microscopy.* e LS, 2001.
16. Neumann, B., M. Held, U. Liebel, H. Erfle, P. Rogers, R. Pepperkok, and J. Ellenberg, *High-throughput RNAi screening by time-lapse imaging of live human cells.* Nature methods, 2006. **3**(5): p. 385.
17. Ohta, J., Y. Ohta, H. Takehara, T. Noda, K. Sasagawa, T. Tokuda, M. Haruta, T. Kobayashi, Y.M. Akay, and M. Akay, *Implantable microimaging device for observing brain activities of rodents.* Proc. IEEE, 2017. **105**(1): p. 158-166.
18. Takehara, H., Y. Katsuragi, Y. Ohta, M. Motoyama, H. Takehara, T. Noda, K. Sasagawa, T. Tokuda, and J. Ohta, *Implantable micro-optical semiconductor devices for optical theranostics in deep tissue.* Appl. Phys. Express, 2016. **9**(4): p. 047001.
19. Haruta, M., N. Kamiyama, S. Nakajima, M. Motoyama, M. Kawahara, Y. Ohta, A. Yamasaki, H. Takehara, T. Noda, and K. Sasagawa, *Implantable optogenetic device with CMOS IC technology for simultaneous optical measurement and stimulation.* Japanese Journal of Applied Physics, 2017. **56**(5): p. 057001.
20. Takehara, H., Y. Ohta, M. Motoyama, M. Haruta, M. Nagasaki, H. Takehara, T. Noda, K. Sasagawa, T. Tokuda, and J. Ohta, *Intravital fluorescence imaging of mouse brain using implantable semiconductor devices and epi-illumination of biological tissue.* Biomed. Opt. Express, 2015. **6**(5): p. 1553-1564.
21. Förster, T., *Zwischenmolekulare energiewanderung und fluoreszenz.* Ann. Phys. (Berl.), 1948. **437**(1-2): p. 55-75.
22. Zheng, J., *FRET and its biological application as a molecular ruler*, in *Biomedical applications of biophysics*. 2010, Springer. p. 119-136.
23. Jares-Erijman, E.A. and T.M. Jovin, *FRET imaging.* Nature biotechnology, 2003. **21**(11): p. 1387.
24. Jares-Erijman, E.A. and T.M. Jovin, *Imaging molecular interactions in living cells by FRET microscopy.* Curr. Opin. Chem. Biol., 2006. **10**(5): p. 409-416.
25. Tsien, R.Y., *The green fluorescent protein*, 1998, Annual Reviews 4139 El Camino Way, PO Box 10139, Palo Alto, CA 94303-0139, USA.
26. Stryer, L., *Fluorescence energy transfer as a spectroscopic ruler.* Annual review of biochemistry, 1978. **47**(1): p. 819-846.
27. Yoshizaki, H., Y. Ohba, K. Kurokawa, R.E. Itoh, T. Nakamura, N. Mochizuki, K. Nagashima, and M. Matsuda, *Activity of Rho-family GTPases during cell division as visualized with FRET-based probes.* J Cell Biol, 2003. **162**(2): p. 223-232.
28. Komatsu, N., K. Aoki, M. Yamada, H. Yukinaga, Y. Fujita, Y. Kamioka, and M. Matsuda,

Development of an optimized backbone of FRET biosensors for kinases and GTPases. Molecular biology of the cell, 2011. **22**(23): p. 4647-4656.

29. Kitano, M., M. Nakaya, T. Nakamura, S. Nagata, and M. Matsuda, *Imaging of Rab5 activity identifies essential regulators for phagosome maturation.* Nature, 2008. **453**(7192): p. 241.
30. Aoki, K., N. Komatsu, E. Hirata, Y. Kamioka, and M. Matsuda, *Stable expression of FRET biosensors: a new light in cancer research.* Cancer science, 2012. **103**(4): p. 614-619.
31. Kiyokawa, E., S. Hara, T. Nakamura, and M. Matsuda, *Fluorescence (Förster) resonance energy transfer imaging of oncogene activity in living cells.* Cancer science, 2006. **97**(1): p. 8-15.
32. Tian, H., L. Ip, H. Luo, D. Chang, and K. Luo, *A high throughput drug screen based on fluorescence resonance energy transfer (FRET) for anticancer activity of compounds from herbal medicine.* British journal of pharmacology, 2007. **150**(3): p. 321-334.
33. Kamioka, Y., K. Sumiyama, R. Mizuno, Y. Sakai, E. Hirata, E. Kiyokawa, and M. Matsuda, *Live imaging of protein kinase activities in transgenic mice expressing FRET biosensors.* Cell structure and function, 2012: p. 1201200102-1201200102.
34. Mizuno, R., Y. Kamioka, Y. Sakai, and M. Matsuda, *Visualization of signaling molecules during neutrophil recruitment in transgenic mice expressing FRET biosensors*, in *Gastrointestinal Physiology and Diseases*. 2016, Springer. p. 149-160.
35. Aoki, K. and M. Matsuda, *Visualization of small GTPase activity with fluorescence resonance energy transfer-based biosensors.* Nature protocols, 2009. **4**(11): p. 1623.
36. Periasamy, A., *Fluorescence resonance energy transfer microscopy: a mini review.* Journal of biomedical optics, 2001. **6**(3): p. 287-292.
37. Hirata, E. and E. Kiyokawa, *Future perspective of single-molecule FRET biosensors and intravital FRET microscopy.* Biophysical journal, 2016. **111**(6): p. 1103-1111.
38. Chai, L., J. Zhang, L. Zhang, and T.-s. Chen, *Miniature fiber optic spectrometer-based quantitative fluorescence resonance energy transfer measurement in single living cells.* Journal of biomedical optics, 2015. **20**(3): p. 037008.
39. Ohayon, S., A. Caravaca-Aguirre, R. Piestun, and J.J. DiCarlo, *Minimally invasive multimode optical fiber microendoscope for deep brain fluorescence imaging.* Biomedical optics express, 2018. **9**(4): p. 1492-1509.
40. Hee, W.S., K. Sasagawa, A. Kameyama, A. Kimura, M. Haruta, T. Tokuda, and J. Ohta, *Lens-free Dual-color Fluorescent CMOS Image Sensor for Förster Resonance Energy Transfer Imaging.* Sensors and Materials, 2019. **31**(8): p. 2579-2594.
41. Solhusvik, J., T. Willassen, S. Mikkelsen, M. Wilhelmsen, S. Manabe, D. Mao, Z. He, K. Mabuchi, and T. Hasegawa, *A 1280x960 2.8 μm HDR CIS with DCG and Split-Pixel*

Combined.

42. Li, J., H. Ebendorff-Heidepriem, B.C. Gibson, A.D. Greentree, M.R. Hutchinson, P. Jia, R. Kostecki, G. Liu, A. Orth, and M. Ploschner, *Perspective: Biomedical sensing and imaging with optical fibers—Innovation through convergence of science disciplines.* APL photonics, 2018. **3**(10): p. 100902.
43. Bigas, M., E. Cabruja, J. Forest, and J. Salvi, *Review of CMOS image sensors.* Microelectronics journal, 2006. **37**(5): p. 433-451.
44. Cevik, I., X. Huang, H. Yu, M. Yan, and S. Ay, *An ultra-low power CMOS image sensor with on-chip energy harvesting and power management capability.* Sensors, 2015. **15**(3): p. 5531-5554.
45. Seo, M.-W., K. Yasutomi, K. Kagawa, and S. Kawahito, *A Low Noise CMOS Image Sensor with Pixel Optimization and Noise Robust Column-parallel Readout Circuits for Low-light Levels.* ITE Transactions on Media Technology and Applications, 2015. **3**(4): p. 258-262.
46. Ohta, J., T. Tokuda, K. Sasagawa, and T. Noda, *Implantable CMOS biomedical devices.* Sensors, 2009. **9**(11): p. 9073-9093.
47. Maruyama, Y., K. Sawada, H. Takao, and M. Ishida, *The fabrication of filter-less fluorescence detection sensor array using CMOS image sensor technique.* Sensors and Actuators A: Physical, 2006. **128**(1): p. 66-70.
48. Yoon, H.-J., S. Itoh, and S. Kawahito, *A CMOS image sensor with in-pixel two-stage charge transfer for fluorescence lifetime imaging.* IEEE Transactions on Electron Devices, 2009. **56**(2): p. 214-221.
49. Lambert, T.J., *FPbase: A community-editable fluorescent protein database.* Nature methods, 2019: p. 1.
50. Sasagawa, K., K. Ando, T. Kobayashi, T. Noda, T. Tokuda, S.H. Kim, R. Iino, H. Noji, and J. Ohta, *Complementary metal–oxide–semiconductor image sensor with microchamber array for fluorescent bead counting.* Japanese Journal of Applied Physics, 2012. **51**(2S): p. 02BL01.
51. Fan, D., D. Rich, T. Holtzman, P. Ruther, J.W. Dalley, A. Lopez, M.A. Rossi, J.W. Barter, D. Salas-Meza, and S. Herwik, *A wireless multi-channel recording system for freely behaving mice and rats.* PloS one, 2011. **6**(7): p. e22033.
52. Haruta, M., C. Kitsumoto, Y. Sunaga, H. Takehara, T. Noda, K. Sasagawa, T. Tokuda, and J. Ohta, *An implantable CMOS device for blood-flow imaging during experiments on freely moving rats.* Japanese Journal of Applied Physics, 2014. **53**(4S): p. 04EL05.
53. Khiarak, M.N., E. Martianova, C. Bories, S. Martel, C.D. Proulx, Y. De Koninck, and B. Gosselin, *A Wireless Fiber Photometry System Based on a High-Precision CMOS Biosensor With Embedded Continuous-Time $\Sigma\Delta $ Modulation.* IEEE

transactions on biomedical circuits and systems, 2018. **12**(3): p. 495-509.
54. Henderson, R.K., N. Johnston, H. Chen, D.D.-U. Li, G. Hungerford, R. Hirsch, D. McLoskey, P. Yip, and D.J. Birch. *A 192× 128 time correlated single photon counting imager in 40nm CMOS technology*. in *ESSCIRC 2018-IEEE 44th European Solid State Circuits Conference (ESSCIRC)*. 2018. IEEE.

Appendix A: Source code for wireless module

```
#include <xc.h>
#include <stdio.h>

#define _XTAL_FREQ  8000000

#pragma config FOSC = INTOSC
#pragma config WDTE = OFF
#pragma config PWRTE = ON
#pragma config MCLRE = OFF
#pragma config CP = OFF
#pragma config BOREN = ON
#pragma config CLKOUTEN = OFF
#pragma config IESO = OFF
#pragma config FCMEN = OFF

#pragma config WRT = OFF
#pragma config PLLEN = OFF
#pragma config STVREN = ON
#pragma config BORV = HI
#pragma config LVP = OFF




void Wait(unsigned int num)
{
    int i ;


    for (i=0 ; i<num ; i++) {
        __delay_ms(10) ;
    }
}
```

```
void main()
{
    char i;
    int var,var2;
    int j,k;
    char buf[4]={0};

     OSCCON = 0b01110010 ;
     ANSELA = 0b00000001 ;
     TRISA  = 0b00000101 ;
     PORTA  = 0b00000000 ;

     ADCON0 = 0;
     ADCON1 = 0x90;

     RC3PPS = 0b10100 ;
     TX1STA  = 0b00100100 ;
     RC1STA  = 0b10010000 ;
     SYNC = 0;
     BRGH = 0;
     BRG16 = 0;
     SPBRG  = 12 ;


     Wait(500) ;
     i = 0x30 ;
     j = 0;
     k=0;


   while(1) {
       for(k=0;k<30;k++){
       for(j=0;j<16;j++){
           RA4 = 1 ;
           RA4 = 0 ;
```

```
          RA4 = 1 ;
          RA4 = 0 ;
          RA4 = 1 ;
          RA4 = 0 ;
          RA4 = 1 ;
          RA4 = 0 ;


        ADCON0 = 0b00000001 ; // AD0
        __delay_us(20);
        ADCON0bits.GO = 1;
        while (ADCON0bits.GO);


        var = ADRESL;
        var2 = ADRESH;
        var = (var2*256+var)/2;


        while(TRMT==0) ;
        while(RA2==0) ;
        TX1REG = var;

      }
        for(j=0;j<64*3;j++){
          RA4 = 1 ;
          RA4 = 0 ;
        }
      }

        for(j=0;j<64*15;j++){
          RA4 = 1 ;
          RA4 = 0 ;
        }

    }
}
```

List of Publications

Journal Article

[1] Wan Shen Hee, Kiyotaka Sasagawa, Aiki Kameyama, Ayaka Kimura, Makito Haruta, Takashi Tokuda, and Jun Ohta. "Lens-free Dual-color Fluorescent CMOS Image Sensor for Förster Resonance Energy Transfer Imaging." Sensors and Materials 31, no. 8 (2019): 2579-2594.

International Conference

[1] Wan Shen Hee, Kenta Nakamoto, Makito Haruta, Toshihiko Noda, Kiyotaka Sasagawa, Takashi Tokuda, Jun Ohta, "Small and Compact In-vivo FRET Image Sensor – Fabrication and Development using CMOS Technology", SSDM 2018, 9-13 September 2018.

Domestic Conference

[1] Wan Shen Hee, Makito Haruta, Toshihiko Noda, Kiyotaka Sasagawa, Takashi Tokuda, Jun Ohta, "Fabrication of a Prototype Dual Filter CMOS Image Sensor for FRET Imaging", *応用物理学会春季学術講演会*, 14-17 March 2017, パシフィコ横浜.

[2] Wan Shen Hee, Kenta Nakamoto, Makito Haruta, Toshihiko Noda, Kiyotaka Sasagawa, Takashi Tokuda, Jun Ohta, "Fabrication of A Small, Compact, Dual Color Prototype FRET

Image Sensor", *LSI とシステムのワークショップ2017*, 15-16 May 2017, 東京大学　生産技術研究所.

[3] Wan Shen Hee, Makito Haruta, Toshihiko Noda, Kiyotaka Sasagawa, Takashi Tokuda, Jun Ohta, "A Dual Color CMOS Image Sensor for In-Vivo FRET Imaging", *映像情報メディア学会 年次大会 2017*, 30 August – 1 September 2017, 東京理科大学 葛飾キャンパス.

[4] Wan Shen Hee, Aiki Kameyama, Makito Haruta, Toshihiko Noda, Kiyotaka Sasagawa, Takashi Tokuda, Jun Ohta "Fabrication of a Thin, High Performance Optical Structure for FRET Imaging", *平成 30 年度 E 部門総合研究会*, 12-13 July 2018, 奈良県文化会館.

[5] Wan Shen Hee, Aiki Kameyama, Ayaka Kimura, Kiyotaka Sasagawa, Makito Haruta, Takashi Tokuda, Jun Ohta, "Application of High Performance Hybrid Filter on CMOS Image Sensor for FRET Imaging", *応用物理学会春季学術講演会*, 9-12 March 2019, 東工大　大岡山キャンパス.